The Astrophysical Journal, 705:89–111, 2009 November 1 doi:10.1088/0004-637X/705/1/89

EXPLORATIONS BEYOND THE SNOW LINE: *SPITZER*/IRS SPECTRA OF DEBRIS DISKS AROUND SOLAR-TYPE STARS

S. M. Lawler[1,2,7], C. A. Beichman[2], G. Bryden[3], D. R. Ciardi[2], A. M. Tanner[3], K. Y. L. Su[4], K. R. Stapelfeldt[3], C. M. Lisse[5], and D. E. Harker[6]

[1] Astronomy Department, Wesleyan University, Middletown, CT 06459, USA
[2] NASA Exoplanet Science Institute, California Institute of Technology, Pasadena, CA 91125, USA
[3] Jet Propulsion Laboratory, 4800 Oak Grove Drive, Pasadena, CA 91109, USA
[4] Steward Observatory, University of Arizona, 933 North Cherry Avenue, Tucson, AZ 85721, USA
[5] Johns Hopkins University - Applied Physics Laboratory, SD/SRE, MP3-W155, 7707 Montpelier Road, Laurel, MD 20723, USA
[6] Center for Astrophysics and Space Sciences, University of California, San Diego, 9500 Gilman Drive, La Jolla, CA 92093-0424, USA
Received 2008 November 13; accepted 2009 September 11; published 2009 October 7

ABSTRACT

We have observed 152 nearby solar-type stars with the Infrared Spectrometer (IRS) on the *Spitzer Space Telescope*. Including stars that met our criteria but were observed in other surveys, we get an overall success rate for finding excesses in the long-wavelength IRS band (30–34 μm) of 11.8% $\pm$ 2.4%. The success rate for excesses in the short-wavelength band (8.5–12 μm) is $\sim$1% including sources from other surveys. For stars with no excess at 8.5–12 μm, the IRS data set 3σ limits of around 1000 times the level of zodiacal emission present in our solar system, while at 30–34 μm data set limits of around 100 times the level of our solar system. Two stars (HD 40136 and HD 10647) show weak evidence for spectral features; the excess emission in the other systems is featureless. If the emitting material consists of large (10 μm) grains as implied by the lack of spectral features, we find that these grains are typically located at or beyond the snow line, $\sim$1–35 AU from the host stars, with an average distance of 14 $\pm$ 6 AU; however, smaller grains could be located at significantly greater distances from the host stars. These distances correspond to dust temperatures in the range $\sim$50–450 K. Several of the disks are well modeled by a single dust temperature, possibly indicative of a ring-like structure. However, a single dust temperature does not match the data for other disks in the sample, implying a distribution of temperatures within these disks. For most stars with excesses, we detect an excess at both IRS and Multiband Imaging Photometer for *Spitzer* (MIPS) wavelengths. Only three stars in this sample show a MIPS 70 μm excess with no IRS excess, implying that very cold dust is rare around solar-type stars.

Key words: infrared: stars – circumstellar matter – planetary systems – Kuiper Belt

Online-only material: color figure, supplementary data file

1. INTRODUCTION

Mid-infrared spectroscopic observations of some young debris stars such as β Pictoris (Telesco & Knacke 1991), 51 Oph (Fajardo-Acosta et al. 1993), and BD+20 307 (HIP 8920; Song et al. 2005) have revealed warm dust composed, at least in part, of small (submicron) grains of crystalline silicates such as forsterite and enstatite. The similarity of these spectral features to those seen in comet C/1995 O1 (Hale-Bopp; e.g., Wooden et al. 2000) suggests that this circumstellar material may represent debris from either cometary or asteroidal material located within the habitable zones of the stars. Dramatically, observations with the Infrared Spectrometer (IRS) on the *Spitzer Space Telescope* (Houck et al. 2004) revealed a bright spectrum of features due to hot (400 K) silicate grains around the nearby (12.6 pc), mature (2 Gyr) K0 V star, HD 69830 (Beichman et al. 2005b). This star, with a level of exo-zodiacal emission $\sim$1400 times that of our own solar system, is also accompanied by a trio of Neptune-mass planets which may be trapping material in an exterior 2:1 resonance at $\sim$1 AU (Lisse et al. 2007). However, these spectral features are not present in all stars with debris disks. More than a dozen classic debris disks, around mostly mature stars (including Fomalhaut), examined by *Spitzer* (Jura et al. 2004; Stapelfeldt et al. 2004) show little or no spectral structure while showing clear excess at these wavelengths. Similarly, most of the other stars with excesses in other surveys with the IRS show no evidence for small grains, suggesting that the grains in these systems are larger than $\sim$10 μm (Beichman et al. 2006a; Chen et al. 2006). These grains may be similar to those in our own zodiacal cloud which are predominantly larger than 10–100 μm with some smaller silicate grains, yielding only a weak 10 μm emission feature (e.g., Reach et al. 2003).

We have used the IRS on *Spitzer* to observe a sample of FGKM stars within 25 pc of the Sun to assess the frequency, amount, and properties of the warm dust located within the habitable zones around solar-like stars. Some stars also have data from the Multiband Imaging Photometer for *Spitzer* (MIPS; Rieke et al. 2004), providing additional information about cool dust located in the Kuiper belts of these systems. This information can shed light on the formation and evolution of circumstellar material located relatively close to the host star.

This study addresses the nature of asteroidal and cometary material, which as the techniques of planet detection improve, may prove to be tracers for gas giant and rocky planets. This is highlighted by the discovery of three planets orbiting in the immediate vicinity of the HD 69830 debris disk (Lovis et al. 2006), as well as by the recent images of an exoplanet within the annulus of Fomalhaut's debris disk (Kalas et al. 2008), and three exoplanets around HR 8799 (Marois et al. 2008), which was previously known to have an IR excess (Rhee et al. 2007). Together with planets, this circumstellar material forms complete

[7] Current address: University of British Columbia, Department of Physics and Astronomy, 6244 Agricultural Road, Vancouver, BC V6T 1Z1 Canada.

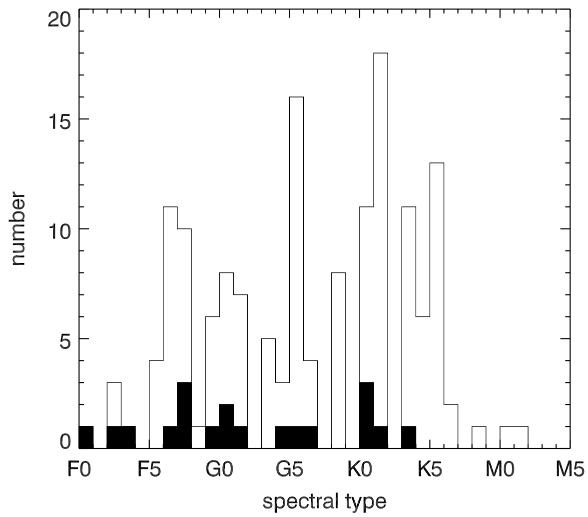

Figure 1. Spectral types of the sample stars. Stars with excesses are noted by filled bars.

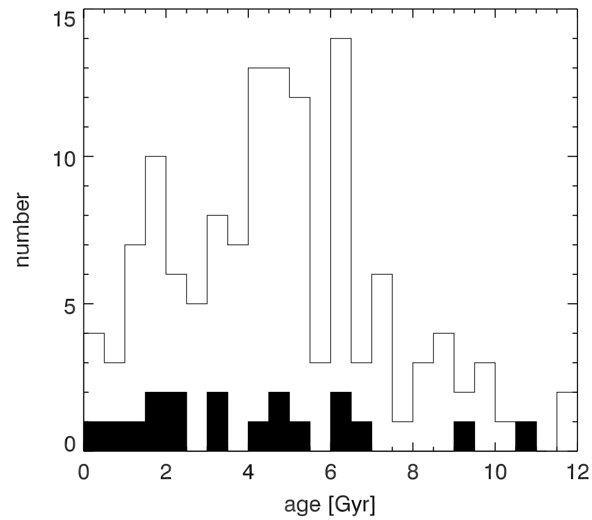

Figure 2. Ages of the sample stars. Stars with excesses are noted by filled bars. Ages are from Wright et al. (2004) or Valenti & Fischer (2005) if available, otherwise we use an average of literature values (see Table 1).

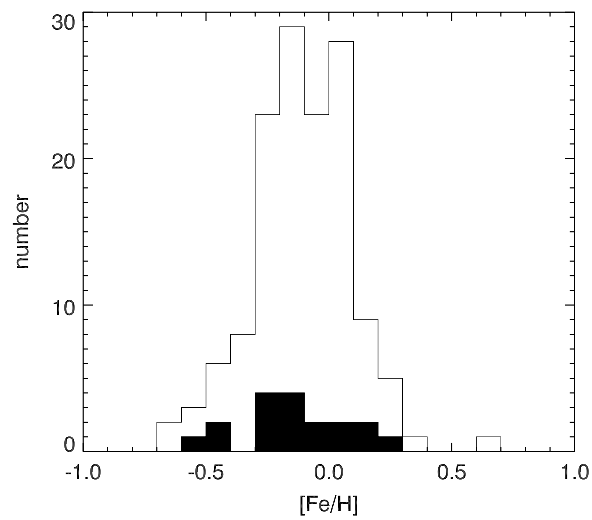

Figure 3. Metallicities of the sample stars. Stars with excesses are noted by filled bars. We use an average of literature values (see Table 1).

planetary systems (Beichman et al. 2007). In this paper, we discuss our sample selection (Section 2), review our reduction procedure and present our spectra (Section 3), discuss measured IR excesses (Section 4), present our models and discuss the nature of the debris disks around 19 stars with detected IRS and/or MIPS 70 μm excesses (Section 5), and review implications of our results for debris disks around solar-type stars (Section 6).

2. THE SAMPLE

The primary goal of our IRS survey is to perform a uniform census of nearby FGKM stars to determine the frequency and amount of warm dust located within the habitable zones of these stars. The survey complements our more complete understanding of the frequency and amount of the cold dust located near the Kuiper Belts of solar-type stars (e.g., Bryden et al. 2006). We have chosen a sample of solar-like stars (spectral types F, G, K, and early M) from the *Hipparcos* data set based upon the following criteria: (1) effective temperature in the range 7300 K $\gtrsim T_{\rm eff} \gtrsim$ 3800 K corresponding to F0–M0 spectral types, (2) luminosity class V, (3) distance within 25 pc of the Sun, (4) no nearby stellar companions, (5) not variable as identified by *Hipparcos* or other catalogs, (6) predicted F_ν(30 μm) flux density of at least 30 mJy, (7) not observed previously by *Spitzer* with the IRS as of 2004 when this sample was defined. This last criterion eliminated 51 stars of which eight have IRS excesses; these numbers have been taken into account in the statistics of detections discussed in Section 4.1. This sample does not include every star that meets these criteria, but stars in the sample have been chosen somewhat randomly, so this should represent an unbiased sample of stars meeting these criteria.

There are 152 stars in the sample, distributed fairly evenly in spectral type. The ends of the distribution are not as well populated, mostly as a result of the distance criterion at the bright end, and the minimum flux density criterion at the faint end. Figures 1–3 show the distribution of stars in spectral type, age, and metallicity, which are listed for each star in Table 1.

The most uncertain stellar parameter is, of course, age, for these mature, main-sequence stars. While the values given in Table 1 (and shown in Figure 2) are derived from many heterogeneous sources, we gave priority to spectroscopic determinations from Wright et al. (2004) or Valenti & Fischer (2005). If not from these two sources, quoted values are an average of a wide variety of values taken from the literature. Thus, the age of any given star must be regarded with caution, i.e., not more accurate than a factor of 2. Of the sample overall, it is safe to say that the vast majority are older than 1 Gyr, well beyond the age when infrared excesses are known to be common among A–G stars (Su et al. 2006; Siegler et al. 2007). HD 10647 highlights the problems with determining ages. Chen et al. (2006) suggest 300 Myr, and the common space motion of this star with the Tucanae–Horologium association lends credence to a young age estimate (Zuckerman & Song 2004). However, Valenti & Fischer (2005) suggest an age around 2–4 Gyr. We use the younger value of 300 Myr.

Of the 152 stars selected, we have MIPS data at 24 μm and 70 μm for 78 stars from a variety of programs (noted in Table 4). These data permit us to cross-correlate the longer wavelength detections of cooler, Kuiper Belt dust with our shorter wavelength detections of hotter dust, yielding a more complete understanding of the dust distribution and mass within exo-zodiacal clouds.

Table 1
Basic Data

Star	HIP	GJ	Spectral Type	Temp. (K)	Distance (pc)	V (mag)	K (mag)	Age W/V/Avg[a] (Gyr)	Age Min (Gyr)	Age Max (Gyr)	Age References	[Fe/H] Average	[Fe/H] σ	[Fe/H] References
HD 870	1031	2001	K0V	5273	20.3	7.22	5.38	2.0	···	···	RP	−0.22	0.06	N,RP
HD 1461	1499	16	G0V	5948	23.4	6.47	4.90	6.3	4.2	9.6	W,V,I,N	0.3	0.1	B,CS,Ce,I,M,N,P,T,Th
HD 1581	1599	17	F9V	6017	8.6	4.23	2.78[b]	5.3	4.1	8.2	V,I,N,RP	−0.2	0.1	CS,E,I,La,M,N,RP,T,Th
HD 3765	3206	28	K2V	5047	17.3	7.36	5.16	7.0	4.8	7.0	V,RP	0.0	0.1	B,CS,I,M,N,P,RP,T
HD 4308[c]	3497	32	G5V	5678	21.9	6.55	4.95	9.5	8.6	9.6	V,I,N,RP	−0.3	0.1	B,CS,I,M,N,RP,T
HD 4813	3909	37	F7IV-V	6226	15.5	5.17	4.02[d]	2.8	1.4	3.8	C,I,La,L,N	−0.14	0.08	B,CS,C,I,La,L,M,N,P,T,Th
HD 5133	4148	42	K3V	4925	14.1	7.15	4.89	6.0	5.4	6.0	V,I	−0.13	0.07	CS,I,M,N,T
HD 7439	5799	54.2 A	F5V	6445	24.4	5.14	4.06[d]	3.0	2.4	4.2	C,L,M,N	−0.31	0.06	B,CS,C,L,M,N,T,Th
HD 8997	6917	58	K2V	5047	23.2	7.74	5.37	···	···	···	···	−0.5	0.1	M,N
HD 9407	7339	59	G6V	5626	21.0	6.52	4.89	5.8	5.6	6.5	W,V,I	0.05	0.03	B,CS,I,M
HD 10360	···	66 B	K0V	5273	6.8	5.76	3.56[d]	3.0	···	···	RP	−0.23	0.03	E,N,RP,T,V
HD 10647[c]	7978	3109	F9V	6017	17.4	5.52	3.29[b]	0.3[e]	0.3	6.3	V,Ch,F,I,N	−0.1	0.1	E,F,I,M,N,T
HD 10780	8362	75	K0V	5273	10.0	5.63	3.84[b]	1.9	0.9	6.8	W,V,La,RP	0.1	0.2	B,CS,Ce,La,M,N,P,RP,T
HD 14412	10798	95	G5V	5678	12.7	6.33	4.55	3.3	3.3	8.0	W,V,La,RP	−0.4	0.4	B,CS,E,I,La,N,RP,T
HD 16673	12444	3175	F6V	6332	21.5	5.79	4.53[d]	2.9	1.6	4.4	C,I,L,N	0.0	0.1	B,CS,C,I,L,M,N,T,Th
HD 16895	12777	107 A	F7V	6226	11.2	4.10	2.98[b]	5.0	1.2	5.0	W,V,C,L,N	−0.06	0.09	B,CS,C,L,M,N,P,T,Th
HD 18803	14150	120	G8V	5484	21.2	6.62	4.95	3.6	3.2	7.9	W,V,I,N	0.13	0.02	B,CS,I,N,T
HD 21197	15919	141	K5V	4557	15.1	7.86	5.12	···	···	···	···	0.31	0.02	CS,I,T
HD 21749	16069	143	K4V	4791	16.4	8.08	5.38	···	···	···	···	···	···	···
HD 23356	17420	···	K2V	5047	14.1	7.10	4.84	6.1	···	···	V	−0.1	···	T
HD 24451	18774	156	K4V	4791	16.0	8.20	5.46	···	···	···	···	···	···	···
HD 24916	18512	157 A	K4V	4791	15.8	8.07	5.34	···	···	···	···	···	···	···
HD 26491	19233	162	G3V	5767	23.2	6.37	4.77[b]	6.4	5.9	12.7	V,I,M,N,RP	−0.18	0.05	B,CS,I,M,N,RP,T,Th
HD 27274	19884	167	K5V	4557	13.1	7.64	4.92	···	···	···	···	···	···	···
HD 28343	20917	169	K7V	4258	11.5	8.30	4.88	···	···	···	···	···	···	···
HD 30501	22122	176	K1V	5156	20.4	7.58	5.53	···	···	···	···	0.0	0.1	CS,I,M,N,T
HD 30652	22449	178	F6V	6332	8.0	3.19	2.20[b]	1.6	1.4	1.7	W,V,N	0.04	0.07	CS,Ce,E,M,N,P,T
HD 32147	23311	183	K3V	4925	8.8	6.22	3.71[d]	5.3	···	···	V	0.2	0.1	CS,I,M,P,T
HD 36003	25623	204	K5V	4557	13.0	7.65	4.88	···	···	···	···	0.09	···	Ce
HD 36395	25878	205	M1.5V	3935	5.7	7.97	4.03[b]	···	···	···	···	0.60	···	CS
HD 38230	27207	217	K0V	5273	20.6	7.34	5.35	5.5	5.2	8.9	W,V,RP	−0.03	0.04	M,N,RP
HD 38392	···	216 B	K2V	5047	9.0	6.15	4.13[d]	0.9	0.9	0.9	La,RP	0.0	0.1	CS,E,La,M,N,RP,T
HD 38393	27072	216 A	F7V	6226	9.0	3.59	2.42[b]	2.0	1.2	2.6	C,La,L,N,RP	−0.05	0.06	Bo,B,CS,Ce,C,E,La,L,Le,M,N,P,RP,T,Th
HD 38858	27435	1085	G4V	5723	15.6	5.97	4.41[d]	4.6	3.2	7.5	W,V,I	−0.24	0.01	B,I,N,T,V
HD 40136	28103	225	F1V	6826	15.0	3.71	2.90[b]	1.3	1.2	1.3	I,N	−0.15	0.06	CS,I,M,N,P
HD 40307[c]	27887	2046	K3V	4925	12.8	7.17	4.79	9.9	···	···	V	−0.26	0.06	N,T
HD 42807	29525	230	G2V	5819	18.1	6.43	4.85	0.4	0.2	0.6	Ba,RP	−0.1	0.1	I,M,N,RP
HD 43042	29650	3390	F6V	6332	21.1	5.20	4.13[d]	1.4	1.1	1.8	V,C,L,M,N	0.04	0.03	B,CS,C,L,M,Ms,N,T,Th
HD 45184	30503	3394	G2IV	5819	22.0	6.37	4.87	4.6	4.1	7.4	W,V,I,M,N	0.01	0.03	B,I,M,N
HD 46588	32439	240	F8V	6115	17.9	5.44	4.14[d]	5.2	4.3	6.2	Ba,F,I,N,RP	−0.22	0.07	F,I,M,N,RP
HD 49095	32366	245	F6V	6332	24.3	5.92	4.66	3.6	3.3	3.9	I,N	−0.2	0.1	I,M,N
HD 50281	32984	250 A	K3V	4925	8.7	6.58	4.11[d]	3.1	2.6	3.1	V,La	0.0	0.1	B,CS,La,M,T,V
HD 50692	33277	252	G0V	5948	17.3	5.74	4.29[d]	4.5	4.5	9.5	W,V,Ba,I,N,RP	−0.26	0.09	E,I,M,N,RP
HD 52711	34017	262	G4V	5723	19.1	5.93	4.53[b]	4.8	4.8	13.9	W,V,Ba,I,L,N,RP	−0.19	0.06	B,CS,E,I,L,M,Ms,N,P,RP,T
HD 53705	34065	264.1 A	G3V	5767	16.2	5.56	4.04[d]	7.2	6.3	12.9	V,N,RP	−0.29	0.09	CS,E,M,N,RP,T,V
HD 59468	36210	275	G5V	5678	22.5	6.72	5.04	8.0	3.5	14.0	V,N,RP	0.06	0.04	M,N,RP

Table 1
(Continued)

Star	HIP	GJ	Spectral Type	Temp. (K)	Distance (pc)	V (mag)	K (mag)	Age W/V/Avg[a] (Gyr)	Age Min (Gyr)	Age Max (Gyr)	Age References	[Fe/H] Average	[Fe/H] σ	[Fe/H] References
HD 62613	38784	290	G8V	5484	17.0	6.55	4.86	3.1	3.1	6.2	W,Ba,N,RP	−0.14	0.03	B,E,I,N,RP
HD 65583	39157	295	G8V	5484	16.8	6.97	5.10	4.8	4.8	10.4	W,V,Ba,RP	−0.63	0.08	CS,Ce,I,Le,M,Ms,N,P,RP,T
HD 65907	38908	294 A	G0V	5948	16.2	5.59	4.24[b]	5.8	4.5	9.6	V,N,RP	−0.38	0.06	CS,N,RP,T
HD 67199	39342	3476	K1V	5156	17.3	7.18	5.12	7.1	2.4	7.1	V,RP	−0.1	0.1	N,RP
HD 68017	40118	9256	G4V	5723	21.7	6.78	5.09	4.2	4.1	11.0	W,V,Ba,N,RP	−0.44	0.05	B,M,Ms,N,RP
HD 68146	40035	297.2 A	F7V	6226	22.5	5.53	4.35[d]	4.2	2.9	5.2	C,L,M,N	−0.12	0.09	B,CS,C,E,L,M,N,T,Th
HD 69897	40843	303	F6V	6332	18.1	5.13	3.92[b]	3.6	3.2	4.7	W,V,C,I,La,L,N	−0.3	0.1	Bo,B,CS,Ce,C,I,La,L,M,N,P,T,Th
HD 71148	41484	307	G5V	5678	21.8	6.32	4.83	4.7	4.6	12.2	W,V,Ba,I,L,N,RP	−0.1	0.1	B,E,I,L,M,N,RP
HD 71243	40702	305	F5III	6445	19.5	4.05	3.15[d]	1.5	1.4	1.5	F,N	0.07	0.02	F,M,N
HD 72673	41926	309	K0V	5273	12.2	6.38	4.44[d]	4.6	4.6	8.1	W,V,RP	−0.37	0.06	CS,E,I,M,N,RP,T,V
HD 72760	42074	3507	G5	5678	21.8	7.32	5.42	0.3	0.3	7.0	W,V	0.01	0.00	B,N
HD 73667	42499	315	K1V	5156	18.5	7.61	5.44	4.9	4.9	7.8	W,V,RP	−0.42	0.09	CS,M,N,RP,T
HD 76653	43797	3519	F6V	6332	24.1	5.70	4.56[d]	2.3	2.1	2.5	I,N	−0.04	0.07	I,M,N
HD 78366	44897	334	F9V	6017	19.1	5.95	4.55	2.5	2.5	6.5	V,I,N	0.02	0.09	B,E,I,M,N,V
HD 82106	46580	349	K3V	4925	12.7	7.20	4.79	4.4	0.4	4.4	V,RP	0.0	0.1	B,I,M,N,RP
HD 84035	47690	365	K5V	4557	17.8	8.13	5.48	...	...	...	...	...	...	...
HD 85512	48331	370	M0V	4045	11.2	7.67	4.72	...	...	...	...	...	...	...
HD 90089	51502	392	F2V	6727	21.5	5.25	4.27[d]	1.8	1.5	2.1	I,N	−0.3	0.1	I,M,N,T
HD 90156	50921	3597	G5V	5678	22.1	6.92	5.25	4.6	4.6	7.8	W,V,N,RP	−0.29	0.00	N,RP
HD 91324	51523	397	F6V	6332	21.9	4.89	3.58[d]	4.5	4.3	4.7	L,M,N	−0.5	0.3	B,CS,L,M,N,P,T,Th
HD 91889	51933	398	F7V	6226	24.6	5.71	4.34[d]	6.4	5.2	7.4	C,L,M,N	−0.26	0.06	B,CS,C,L,M,N,T,Th
HD 97101	54646	414 A	K8V	4258	11.9	8.31	4.98	...	...	...	...	...	...	...
HD 98281	55210	423	G8V	5484	22.0	7.29	5.46	4.5	4.5	8.5	W,V	−0.2	0.1	M,N
HD 100180	56242	3669 A	G0V	5948	23.0	6.27	4.90	4.5	3.4	9.2	W,V,C,L,N	−0.11	0.05	CS,C,L,M,N,T
HD 100623	56452	432 A	K0V	5273	9.5	5.96	4.02[d]	3.7	3.7	7.8	W,V,La,RP	−0.4	0.1	E,La,M,N,RP,T,V
HD 102438	57507	446	G5V	5678	17.8	6.48	4.80	9.7	6.4	9.7	V,N,RP	−0.2	0.2	I,M,N,RP,T
HD 103932	58345	453	K5V	4557	10.2	6.99	4.53[d]	...	...	...	...	0.16	0.00	CS,I,T
HD 104067	58451	1153	K2V	5047	20.8	7.92	5.61	7.5	...	...	V	...	...	...
HD 104731	58803	3701	F6V	6332	24.2	5.15	4.09[b]	2.0	1.7	2.4	F,I,L,M,N	−0.17	0.05	CS,F,I,L,M,N,Th
HD 108954	61053	...	F9V	6017	21.9	6.20	4.82	4.0	3.8	4.2	I,N	−0.10	0.06	B,CS,I,M,N,T,Th
HD 109200	61291	472	K1V	5156	16.2	7.13	5.07	10.0	3.6	10.0	V,RP	−0.2	0.2	M,N,RP
HD 109524	61451	1161 A	K5V	4557	21.6	7.84	5.26	...	...	...	...	...	...	...
HD 110810	62229	...	K3V	4925	20.1	7.82	5.61	7.3	...	...	V	...	...	...
HD 110897	62207	484	G0V	5948	17.4	5.95	4.52[b]	9.4	4.9	14.5	Ba,C,I,N	−0.5	0.1	Bo,B,CS,Ce,C,I,M,N,P,T,Th
HD 111395	62523	486	G7V	5560	17.2	6.29	4.65[d]	1.2	1.2	13.3	W,V,N	0.00	0.02	E,M,N
HD 113194	64618	...	K5V	4557	17.6	8.35	5.26	...	...	...	...	...	...	...
HD 114710	64394	502	F9.5V	6017	9.2	4.23	2.89[b]	2.3	1.7	9.6	W,V,Ba,C,La,L,N	0.05	0.08	Bo,CS,Ce,C,La,L,Le,M,Ms,N,P,T,Th
HD 115617	64924	506	G5V	5678	8.5	4.74	2.96[d]	6.3	6.3	12.3	W,La,N	0.00	0.03	Bo,CS,Ce,E,La,M,N,T,Th
HD 117043	65530	511	G6V	5626	21.3	6.50	4.80	10.8	...	...	N	0.16	0.08	B,N
HD 120690	67620	530	G5V	5678	19.9	6.43	4.67[d]	2.2	2.2	11.4	W,V,I,N,RP	−0.09	0.07	CS,E,I,N,RP,T
HD 121560	68030	...	F6V	6332	24.2	6.16	4.84	4.2	4.2	8.7	W,V,C,I,L,N	−0.37	0.07	B,CS,C,I,L,M,Ms,N,T
HD 122064	68184	...	K3V	4925	10.1	6.49	4.09[d]	6.9	...	...	V	0.07	...	B
HD 124580	69671	540	F9V	6017	21.0	6.31	4.89	5.0	1.2	10.1	I,N,RP	−0.2	0.1	I,M,N,RP
HD 126053	70319	547	G1V	5870	17.6	6.25	4.64[b]	4.6	3.5	14.4	W,V,Ba,I,N,RP	−0.3	0.1	B,CS,I,Le,M,Ms,N,RP
HD 128165	71181	556	K3V	4925	13.4	7.24	4.79	7.1	1.4	7.1	V,RP	0.07	0.06	M,N,RP
HD 128400	71855	3863	G5V	5678	20.3	6.73	5.07	8.2	0.9	15.4	N,RP	−0.07	0.04	N,RP

Table 1
(Continued)

Star	HIP	GJ	Spectral Type	Temp. (K)	Distance (pc)	V (mag)	K (mag)	Age W/V/Avg[a] (Gyr)	Age Min (Gyr)	Age Max (Gyr)	Age References	[Fe/H] Average	[Fe/H] σ	[Fe/H] References
HD 128987	71743	···	G6V	5626	23.6	7.24	5.53	4.3	···	···	N	0.04	0.02	CS,N,T
HD 129502	71957	9491	F2III	6727	18.7	3.87	2.90[b]	1.3	0.7	1.7	F,I,M,N	0.03	0.09	F,I,M,N
HD 130992	72688	565	K3V	4925	17.0	7.81	5.39	6.0	···	···	V	0.0	0.1	M,N
HD 131977	73184	570 A	K4V	4791	5.9	5.72	3.15[b]	3.3	0.4	3.3	V,RP	0.05	0.06	CS,Ce,Le,P,RP,T,V
HD 132254	73100	3880	F7V	6226	24.8	5.63	4.41	3.4	2.2	4.0	C,F,I,L,M,N	0.02	0.05	B,CS,C,F,I,L,M,N,T
HD 134060	74273	···	G2V	5819	24.1	6.29	4.84	3.8	3.8	9.6	V,F,I,M,N,RP	−0.03	0.09	F,I,M,N,RP
HD 134083	73996	578	F5V	6445	19.7	4.93	3.88[b]	1.6	1.3	1.8	V,La,N	0.01	0.08	CS,Ce,E,La,M,N,T,Th
HD 135599	74702	···	K0	5273	15.6	6.92	4.96	1.0	1.0	6.6	W,V	−0.12	···	B
HD 142709	78170	604	K4V	4791	14.7	8.06	5.28	···	···	···	···	···	···	···
HD 142860	78072	603	F6IV	6332	11.1	3.85	2.62[b,d]	2.9	2.9	5.5	W,C,L,M,N	−0.18	0.05	CS,Ce,C,La,L,M,N,P,T,Th
HD 144579	78775	611 A	G8V	5484	14.4	6.66	4.76	5.0	5.0	11.6	W,V,Ba,RP	−0.63	0.09	B,I,M,Ms,N,RP
HD 145825	79578	···	G1V	5870	21.9	6.55	5.00	4.5	0.2	4.5	V,M,N,RP	0.18	0.02	M,N,RP
HD 149661	81300	631	K2V	5047	9.8	5.77	3.86[b]	1.2	1.2	4.3	W,V,La	0.1	0.2	B,CS,Ce,E,La,M,N,P,T
HD 151288	82003	638	K5	4557	9.8	8.10	4.71	···	···	···	···	···	···	···
HD 154345[c]	83389	651	G8V	5484	18.1	6.76	5.00	4.0	4.0	6.7	W,V,Ba,RP	−0.11	0.07	B,CS,I,M,N,RP,T
HD 154363	83591	653	K5V	4557	10.8	7.70	4.73	···	···	···	···	···	···	···
HD 154577	83990	656	K2V	5047	13.7	7.38	5.09	6.6	···	···	V	−0.5	0.1	M,N
HD 156026	84478	664	K5V	4557	6.0	6.33	3.47[d]	0.6	···	···	La	−0.20	0.09	CS,La,Le,P,T,Th
HD 157214	84862	672	G0V	5948	14.4	5.38	3.91[d]	6.5	6.5	12.5	W,V,Ba,N	−0.38	0.04	B,CS,Ce,La,M,Ms,N,P,T,Th
HD 157347	85042	···	G5IV	5678	19.5	6.28	4.69	6.3	4.0	13.2	W,V,C,I,L,N,R	0.00	0.03	B,CS,C,I,L,N,R,T
HD 157881	85295	673	K5	4557	7.7	7.54	4.14[b]	5.3	···	···	La	0.1	0.3	CS,Ce,I
HD 158633	85235	675	K0V	5273	12.8	6.44	4.52[d]	4.3	4.3	7.8	W,V	−0.44	0.07	B,E,I,M,N,V
HD 160032	86486	686	F3IV	6628	21.9	4.76	3.83[d]	2.4	1.9	3.3	F,I,M,N	−0.28	0.06	B,CS,F,I,M,N,T,Th
HD 162004	86620	694.1 B	G0V	5948	22.3	5.81	4.53[d]	5.4	4.2	6.1	Ba,C,L,M,N,RP	−0.1	0.1	B,CS,C,L,M,N,RP,T,Th
HD 164259	88175	699	F2IV	6727	23.2	4.62	3.64[d]	1.8	1.3	2.1	F,I,L,M,N	−0.10	0.06	CS,Ce,F,I,L,M,N
HD 164922[c]	88348	700	K0V	5273	21.9	7.01	5.11	6.6	3.7	10.7	W,V,Ba,RP	0.11	0.07	B,M,RP
HD 165401	88622	702	G0V	5948	24.4	6.80	5.25	6.0	1.3	14.2	Ba,I,N,RP	−0.46	0.04	B,CS,Ce,I,M,N,RP,T,Th
HD 168009	89474	708	G2V	5819	22.7	6.30	4.76	7.4	6.4	12.8	W,V,Ba,C,I,L,N,RP	−0.06	0.04	B,CS,C,I,L,Ms,N,RP,T
HD 170493	90656	715	K3V	4925	18.8	8.04	5.48	6.4	···	···	V	0.27	···	M
HD 170657	90790	716	K1V	5156	13.2	6.81	4.70	1.6	1.6	6.1	W,V	0.27	···	M
HD 172051	91438	722	G5V	5678	13.0	5.85	4.23	3.9	1.5	8.5	W,V,I,RP	−0.27	0.03	B,E,I,N,RP,V
HD 177565	93858	744	G5IV	5678	17.2	6.15	4.54[d]	5.4	2.5	13.2	V,I,N,R,RP	0.05	0.02	B,CS,E,I,N,R,RP,T,Th,V
HD 182488	95319	758	G8V	5484	15.5	6.37	4.49[d]	4.5	4.1	10.5	W,V,I,RP	0.11	0.08	B,E,I,M,N,RP,V
HD 183870	96085	1240	K2V	5047	18.0	7.53	5.33	6.1	···	···	V	−0.15	···	N
HD 184385	96183	762	G5V	5678	20.2	6.89	5.17	1.2	1.1	3.9	W,V	0.04	0.04	B,N
HD 185144	96100	764	K0V	5273	5.8	4.67	2.78[b,d]	3.2	3.2	9.2	W,V,Ba,La	−0.3	0.1	CS,La,Le,M,N,P,T
HD 189245	98470	773	F7V	6226	20.9	5.65	4.48[d]	4.2	3.2	5.2	I,N	−0.26	0.07	I,M,N
HD 189567	98959	776	G3V	5767	17.7	6.07	4.51[d]	8.9	5.0	15.1	V,I,N,RP	−0.29	0.06	CS,I,M,N,P,RP,T,Th
HD 190404	98792	778	K1V	5156	15.6	7.28	5.11	5.1	5.1	9.8	W,V,RP	−0.3	0.2	CS,I,Le,N,P,RP,T,Th
HD 190406	98819	779	G1V	5870	17.7	5.80	4.39[d]	2.5	2.5	8.8	W,V,Ba,M,N,RP	−0.04	0.05	B,CS,Ce,E,M,N,RP,V
HD 190470	98828	779	K3V	4925	21.6	7.82	5.64	···	···	···	···	0.17	···	M
HD 191785	99452	783.2 A	K1V	5156	20.5	7.34	5.35	6.2	6.2	9.5	W,V	−0.19	···	M
HD 191849	99701	784	K7	4258	6.2	7.97	4.28[b]	···	···	···	···	···	···	···
HD 192310	99825	785	K0Vvar	5273	8.8	5.73	3.50[d]	9.3	9.3	10.2	V,I	0.0	0.1	CS,Ce,E,I,N,P,T,Th,V
HD 193664	100017	788	G3V	5767	17.6	5.91	4.45	4.7	4.6	11.7	V,Ba,I,L,M,N,RP	−0.1	0.1	B,CS,I,L,M,N,P,RP,T
HD 197076	102040	797 A	G5V	5678	21.0	6.43	4.92	4.2	4.2	11.4	W,V,Ba,N,RP	−0.2	0.1	B,Ce,M,N,RP

Table 1
(Continued)

Star	HIP	GJ	Spectral Type	Temp. (K)	Distance (pc)	V (mag)	K (mag)	Age				[Fe/H]		
								W/V/Avg[a] (Gyr)	Min (Gyr)	Max (Gyr)	References	Average	σ	References
HD 197692	102485	···	F5V	6445	14.7	4.13	3.09[d]	2.0	1.7	2.3	I,La,N	−0.03	0.07	CS,I,La,M,N,T,Th
HD 199260	103389	811	F7V	6226	21.0	5.70	4.48[d]	3.2	2.9	3.5	I,N	−0.2	0.1	I,M,N
HD 205390	106696	833	K2V	5047	14.7	7.14	4.97	6.3	···	···	V	−0.22	0.09	M,N
HD 205536	107022	···	G8V	5484	22.1	7.07	5.27	8.9	4.0	9.1	V,N,RP	−0.06	0.04	N,RP
HD 210302	109422	849	F6V	6332	18.7	4.94	3.70[d]	5.4	1.4	5.4	W,V,I,L,M,N	0.02	0.06	CS,I,L,M,N,T
HD 210918	109821	851	G5V	5678	22.1	6.23	4.66[d]	8.5	3.9	10.6	V,I,M,N,RP	−0.1	0.1	B,CS,I,M,N,RP,T
HD 212168	110712	···	G3V	5767	23.0	6.12	4.71[d]	4.8	4.4	12.0	V,M,N,RP	−0.16	0.08	M,N,RP
HD 213042	110996	862	K5V	4557	15.4	7.65	5.12	···	···	···	···	0.24	0.01	CS,I,T
HD 213845	111449	863	F7V	6226	22.7	5.21	4.33[b,d]	1.6	1.1	2.3	I,M,N	0.0	0.1	I,M,N,T
HD 218511	114361	1279	K5V	4557	15.1	8.29	5.33	···	···	···	···	···	···	···
HD 219623	114924	4324	F7V	6226	20.3	5.58	4.31[d]	5.1	4.6	5.5	C,L,M,N	−0.04	0.09	B,CS,Ce,C,E,L,M,N,P,T,Th
HD 221354	116085	895	K2V	5047	16.9	6.76	4.80	11.6	10.5	11.6	V,I	0.01	0.01	I,M
HD 222237	116745	902	K4V	4791	11.4	7.09	4.58	8.8	···	···	V	−0.2	0.1	E,M,N,T,V
HD 222335	116763	902	K1V	5156	18.7	7.18	5.27	8.3	2.3	8.3	V,RP	−0.16	0.04	M,N,RP,T

Notes. Spectral types from SIMBAD. Visual magnitudes are as quoted in SIMBAD, typically from the *Hipparcos* satellite, and K magnitudes are from 2MASS unless otherwise noted.
[a] Age from Wright et al. (2004) or Valenti & Fischer (2005) if available, otherwise an average of literature values.
[b] Star has J, H and/or K values from Johnson et al. (2001) or other literature.
[c] Star has at least one known radial velocity planet.
[d] Star has one or more bad 2MASS values (error > 20%), slightly reducing the accuracy of its photometric model.
[e] After considering several factors, our age for HD 10647 comes from Chen et al. (2006; see note in Section 2). Minimum and maximum ages for this star are from all literature sources.
Reference. B: Borkova & Marsakov 2005; Ba: Barry 1988; Bo: Borges et al. 1995; C: Chen et al. 2001; Ch: Chen et al. 2006; CS: Cayrel de Strobel et al. 1996, 2001; Ce: Cenarro et al. 2001; D: Ducati 2002; E: Eggen 1998; F: Feltzing et al. 2001; I: Ibukiyama & Arimoto 2002; K: Kidger & Martín-Luis 2003; L: Lambert & Reddy 2004; La: Lachaume et al. 1999; Le: Lebreton et al. 1999; M: Marsakov & Shevelev 1988, 1995; Ms: Mashonkina & Gehren 2001; Ml: Morel & Magnenat 1978; N: Nordström et al. 2004; P: Perrin et al. 1977; R: Randich et al. 1999; RP: Rocha-Pinto & Maciel 1998; S: Sylvester & Mannings 2000; T: Taylor 2003; Th: Thevenin 1998; V: Valenti & Fischer 2005; W: Wright et al. 2004.

Table 2
Superflats

Superflat	IRS Campaigns	Programs Included[a]	No. of Stars Using Superflat	No. of Stars Used to Make Superflat
1	1–5	FGK	21	16
2	6–22	FGK, SIM/TPF	30	21
3	25	IRS, SIM/TPF	28	19
4	26–27	IRS, FGK	27	16
5	28	IRS, FGK	27	23
6	29	IRS, FGK, SIM/TPF	35	30
7	30	IRS	25	22
8	31–38	IRS	20	19

Note. [a] IRS refers to this paper, FGK refers to Beichman et al. (2006a), and SIM/TPF refers to Beichman et al. (2006b).

3. OBSERVATIONS AND DATA REDUCTION

We observed each star with all four wavelength modules of the IRS: short-low orders 2 and 3 (SL2; 5.1–7.5 μm, SL3; 7.1–8.4 μm), short-low order 1 (SL1; 7.5–14.0 μm), long-low order 2 (LL2; 14.0–20.5 μm), and long-low order 1 (LL1; 20–34 μm), as part of the *Spitzer* GO program 20463 (PI: D. Ciardi). The basic observing sequence and associated data reduction have been described in Beichman et al. (2005a) and Beichman et al. (2006a). In summary, we have used the fact that the vast majority of the sample (>85%) shows no excess in an initial examination of the IRS data or in longer wavelength MIPS data to derive a "superflat" to improve the relative calibration of all the spectra and thus to make small deviations from expected photospheric levels detectable with the greatest possible sensitivity.

The data reduction procedure started with the Spitzer Science Center-calibrated spectrum, obtained either from images resulting from the subtraction of the two nod positions and extracted using the Spitzer Science Center program *Spice*, or from the default Nod1–Nod2 difference spectra provided by the Spitzer Science Center. The error bars are calculated by combining the errors provided by the SSC with 2% of the photospheric flux at each wavelength. A superflat was created for groups of ∼15–20 stars in nearby IRS campaigns (Table 2), grouping stars by the date their data were taken. Each superflat was derived by taking the ratio of the SSC spectra to Kurucz models (Kurucz 1992) appropriate for the effective temperature and metallicity of each star fitted to near-IR and visible photometry as described in Bryden et al. (2006) and Beichman et al. (2006a). Stars with obvious excesses in the IRS data or with excesses in the MIPS data (when available) were excluded from the superflat. A few objects with problems in the IRS spectra, e.g., another star near the slit or obvious pointing problems, were also rejected. To increase the sample size in making superflats, we used IRS data from this sample and two closely related surveys that were taken at around the same time: the SIM/TPF sample (which surveyed possible target stars for the future Space Interferometry Mission and the Terrestrial Planet Finder; Beichman et al. 2006b), and the FGK sample (which surveyed nearby solar-type stars; Beichman et al. 2006a). Each module was normalized to the photospheric model using a single constant whose value differed from unity by less than 25% with a dispersion of 8%. The spectral data for each star in a group were then divided by the group's superflat at each wavelength, thereby eliminating any of the residual flat-field errors missed by the standard *Spitzer* pipeline reduction, including the "droop" at ∼12 μm which was a significant source of error in some of our brightest stars. As shown in Figure 4, this process produces very uniform spectra, with the average fractional excesses $[F_\nu(\text{Observed}) - F_\nu(\text{Photosphere})]/F_\nu(\text{Photosphere})$ of all the stars used to make the superflats deviating from zero by less than 0.5%.

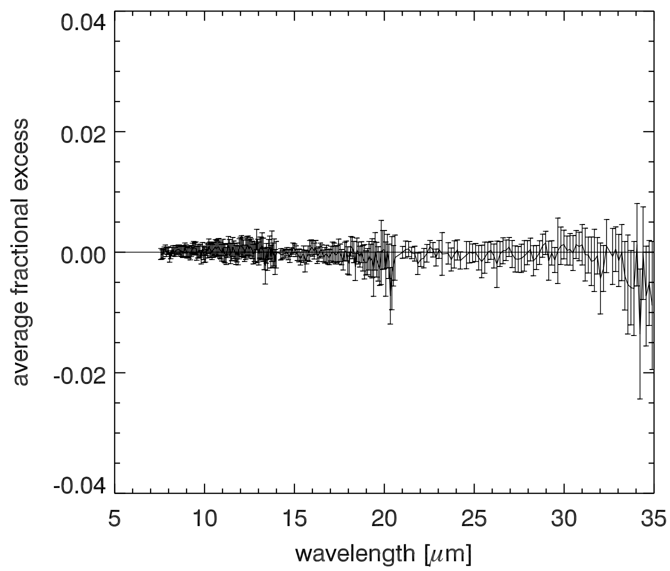

Figure 4. Average fractional excess for 126 stars with no excesses averaged by wavelength. These spectra are beautifully calibrated, with an average deviation from the photosphere of less than 0.5%.

The defining characteristic of the dozens of debris disks we (and others) have examined is an excess that first becomes detectable at some minimum wavelength (typically longward of ∼20 μm, in the IRS LL1 or LL2 modules) and then deviates more and more from the photosphere, rising to longer wavelengths. To look for weak excesses, we calculated a multiplicative calibration factor for each star and each IRS module using the first 10 data points in each module to "pin" the short-wavelength end of each module to the photospheric model. While the origin of these residual gain errors is unknown (errors in the photospheric extrapolation, stellar variability, or residual calibration errors are all possible), the values of this calibration factor are small and uniformly distributed around unity: 1.00 ± 0.07.

Three stars, HD 10360, HD 162004, and HD 185144, had calibration factors significantly outside this range. Examination of Two Micron All Sky Survey (2MASS) images with the IRS slit superimposed showed that HD 10360 and HD 162004 had close companions that were in or close to the IRS slit when data were taken. The AOR for HD 185144 was improperly aligned with the slit, passing over the edge of the star rather than the center, causing the flux to be improperly measured in the SL1 module. There was no evidence of an excess for any of these three stars, albeit at a reduced level of precision (< 5%–10%).

The technique of calibrating each module to the star's photosphere produced smaller residuals and showed no significant deviation from zero over the entire IRS wavelength range for the vast majority of the sample. Defining, for convenience, two "photometric bands" useful for isolating either the silicate features (8.5–12 μm) or a long-wavelength excess (30–34 μm), we see that the dispersion in the deviation from a smooth photosphere was reduced from ∼8% to 1% (8.5–12 μm) and 2% (30–34 μm) when examining non-excess stars. We found no deviation between the stellar photosphere and the IRS data for the majority of the sample, nor did we see any strong evidence of silicate features in any of the stars (8.5–12 μm). We did, however, find clear evidence of excesses longward of ∼15–25 μm for 16 stars and hints of a feature at ∼20 μm for HD 10647 and HD 40136.

In applying our technique we were very careful not to artificially suppress any excess by our method of pinning the short-wavelength end of a module to the photospheric model. For example, for any stars showing even a small excess in LL2 (14–21 μm), we adjusted the short end of LL2 to fit the photosphere, and then adjusted the LL1 spectrum (21–34 μm) to fit the LL2 spectrum in their region of overlap with a single gain term. If the SL1 spectrum (7–14 μm) showed any hint of excess emission (this was only the case for one star: HD 219623), we tied LL1 → LL2 → SL1, and anchored the short-wavelength end of SL1 to the photosphere. In this way, we proceeded from longer to shorter wavelengths ensuring that no potential excess was lost.

Splicing the modules together in this way does not necessarily produce results consistent with other methods of combining the modules. HD 10647, which has the largest fractional excess of any of our sample stars, has its LL1 module spliced to the end of the LL2 module, which gives an excess of 96.4 ± 2.8 mJy in the 30–34 μm band. Chen et al. (2006) found an excess of 114 ± 2 mJy in the same band for this star, implying that these error bars should be inflated when comparing excesses between surveys.

We should note, however, that any excess from very hot dust, with roughly a Rayleigh–Jeans spectrum at IRS wavelengths, would be lost in this procedure. This very hot dust has been invoked to account for a spatially resolved excess at 2.2 μm observed by the Palomar Testbed Interferometer (PTI) and Center for High Angular Resolution Astronomy (CHARA) interferometer (Ciardi et al. 2001; Absil et al. 2006). Thus, we cannot rule out the existence of material much hotter than 1000 K around any of these stars.

Seven stars in the sample had an additional IRS measurement from either the FGK or SIM/TPF samples (Table 3). For each of these stars, we co-added the measured flux at each wavelength, which reduced the noise and allowed us to remove bad pixels. Three of these stars (HD 185144, HD 190406, and HD 222237) have no excess, and this was confirmed by comparing the two separate data sets. Interestingly, HD 185144, which was tagged as a bad measurement because of low SL1 values due to improper slit alignment, also had low SL1 values in its redundant measurement. Out of the remaining four stars, three (HD 115617, HD 158633, and HD 199260) have excesses that were confirmed in the separate data sets, and one star (HD 117043) has a weak excess after co-adding.

Table 3
Stars with Two Observations

Star	AOR	Program[a]	$\chi 32$	Comments
HD 115617	12718080	FGK	3.7	Strong excess
	15998976	This paper	6.4	
	Co-add	This paper	5.3	
HD 117043	12718336	FGK	1.6	Weak excess
	16021248	This paper	4.3	
	Co-add	This paper	2.8	
HD 158633	10272256	SIM/TPF	3.7	Strong excess
	16030208	This paper	4.4	
	Co-add	This paper	4.4	
HD 185144	4024576	FGK	0.7	No excess
	15999744	This paper	0.8	
	Co-add	This paper	0.8	
HD 190406	13473536	SIM/TPF	2.0	No excess
	16001792	This paper	0.0	
	Co-add	This paper	1.0	
HD 199260	10272000	SIM/TPF	5.7	Strong excess
	16003840	This paper	6.1	
	Co-add	This paper	6.3	
HD 222237	13473280	SIM/TPF	−0.2	No excess
	16002304	This paper	0.1	
	Co-add	This paper	−0.1	

Note. [a] FGK refers to Beichman et al. (2006a) and SIM/TPF refers to Beichman et al. (2006b).

3.1. SL2 and SL3 Analysis

We examined the shortest wavelength data (SL2 and the "bonus" order, SL3) using the same technique as described above. We adjusted the SL3 data to fit SL2 and then tied the short-wavelength end of SL2 to the photospheric model. The dispersion (1σ) around fits to the photospheric models is 1% in a photometric band defined between 6 and 6.5 μm and 2% in a photometric band defined between 7.5 and 8 μm. There was no evidence of any excess shortward of 8 μm above the 3σ level.

In performing the fitting, we found that there was a systematic offset between the Kurucz models and *Spitzer* spectra for stars later than K5. Figure 5 shows the fractional excess in the SL2/SL3 wavelength band relative to the Kurucz models pinned to the stellar emission at 5 μm, for four groups of spectral types: F, G, K0–K4, and K5 and later. F and G stars reproduce the Kurucz photospheres very clearly, while early K stars show small deviations (∼1%), and late K and early M stars show greater deviations (>3%). As reported by Bertone et al. (2004), both of the commonly used stellar atmosphere models, Kurucz and NextGen (Hauschildt et al. 1999a, 1999b), fail to accurately match later spectral-type stars. From our analysis here and from previous investigations which used MIPS 24 μm observations of nearby K and M stars (Beichman et al. 2006b; Gautier et al. 2007) and found redder $K_s - [24]$ colors than predicted by theory for both Kurucz and NextGen, it appears that this deviation between model and actual spectra is most severe closer to the near-infrared. Examination of the longer wavelength emission for these later-type stars (IRS modules SL1 and LL1/2, and MIPS data when available) revealed no evidence for longer wavelength excess emission. Thus, we attribute this

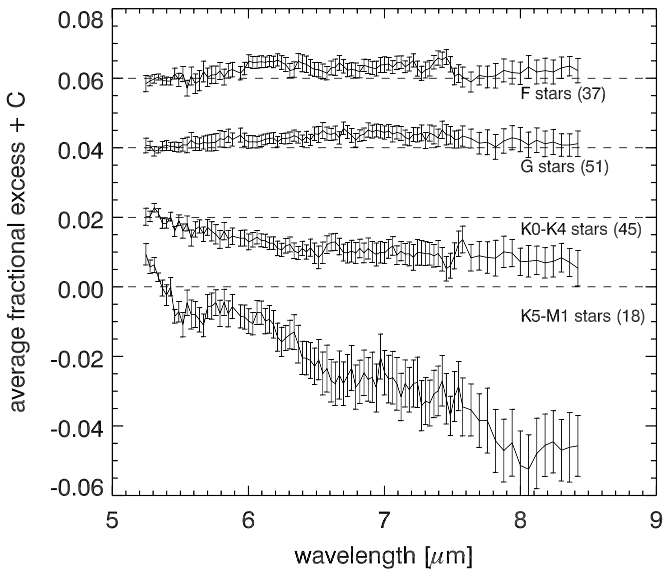

Figure 5. Fractional excess after applying the superflat calibration for 151 stars with valid SL2/SL3 data binned by spectral type. The spectra have been pinned to the photospheric model at 5 μm so deviations show up only at longer wavelengths. The small deviations from zero for the F and G stars demonstrate that the models are very well behaved for these spectral types whereas deviations at the 3%–5% level are apparent at the longest wavelengths for the latest spectral types. Similar deviation from a simple Rayleigh–Jean's extrapolation is seen in the 24 μm photometry of late spectral types (Gautier et al. 2007).

disagreement, resulting in a 5%–10% apparent excess, as due to problems with the photospheric models in the 2–10 μm portion of the spectrum, and not as real excess due to dust emission.

3.2. MIPS Photometry

While the focus of this paper is IRS spectra, for many of our sample stars there is corresponding MIPS photometry at both 24 and 70 μm. Most of these data have already been published; for consistency, we have re-reduced all of them with a uniform set of analysis parameters. Our analysis is similar to that previously described in Beichman et al. (2005a), Bryden et al. (2006), and Beichman et al. (2006b). At 24 μm, images are created from the raw data using software developed by the MIPS instrument team (Gordon et al. 2005), with image flats chosen as a function of scan mirror position to correct for dust spots and with individual frames normalized to remove large-scale gradients (Engelbracht et al. 2007). At 70 μm, images are also processed with the MIPS instrument team pipeline which includes corrections for time-dependent transients (Gordon et al. 2007). Aperture photometry is performed as in Beichman et al. (2005a) with aperture radii of 15.″3 and 14.″8, background annuli of 30.″6–43.″4 and 39.″4–78.″8, and aperture corrections of 1.15 and 1.79 at 24 and 70 μm, respectively. For three systems that are marginally resolved at 70 μm (HD 10647, HD 38858, and HD 115617; see Section 5.2.3), the small aperture fails to capture all of the extended emission; for these three cases the MIPS fluxes listed in Table 5 are based on model fits to each disk (G. Bryden et al. 2009, in preparation). While our procedure has changed little since Bryden et al. (2006) was published, note that improvements in the instrument calibration since then have increased the overall 70 μm flux conversion by 4%, from 15.8 to 16.5 mJy/arcsec^2/MIPS_70_unit (MIPS_70_unit is an internally defined standard based on the ratio of the measured signal to that from the stimulator flash signal (Gordon et al. 2007). Overall, we find no qualitative disagreement between our results and those from earlier publications.

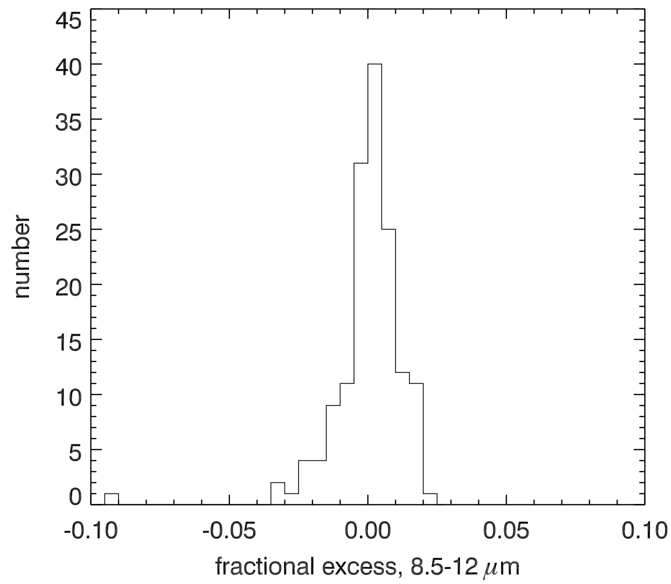

Figure 6. Histogram showing the distribution of fractional excess measured within a photometric band at 8.5–12 μm.

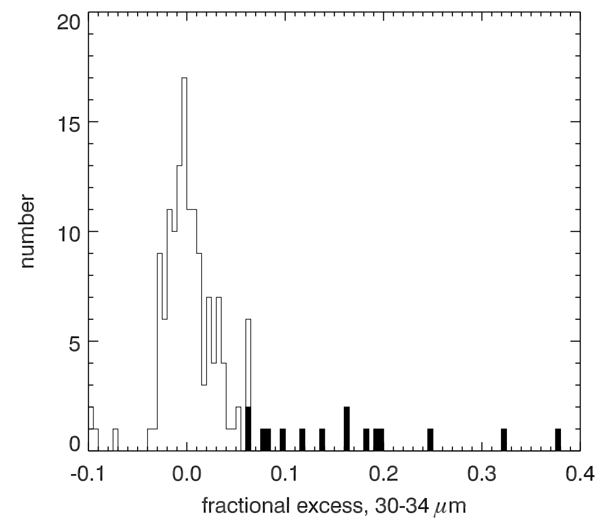

Figure 7. Histogram showing the distribution of fractional excess measured within a photometric band at 30–34 μm. Filled bars represent stars with statistically significant excesses. The point for HD 10647 is off-scale to the right with a fractional excess of 1.2.

4. RESULTS

After flattening and normalizing the IRS spectra as described above, we estimate the fractional excess $[F_\nu(\text{Observed}) - F_\nu(\text{Photosphere})]/F_\nu(\text{Photosphere})$. We will continue to use the two photometric bands previously defined to isolate either the silicate features (8.5–12 μm) or a long-wavelength excess (30–34 μm). Figures 6 and 7 show histograms of the fractional excess measured in these photometric bands. In assessing the significance of an excess, we looked at the internal uncertainty in the flux density measurement of a given star and the fractional excess relative to the $\sim$2% dispersion in the entire sample (Table 4). The amplitude of the fractional excess relative to the entire population is more important in assessing the reality of an excess than the internal signal-to-noise ratio (S/N) in an individual spectrum. There are a number of stars that appear to have a significant excess when looking only at the internal uncertainties, but which are not so impressive

Table 4
IRS Data

Star	8.5–12 μm Excess (mJy)	Fractional Excess	χ10	L_{dust}/L_* [a] ($\times10^{-5}$)	30–34 μm Excess (mJy)	Fractional Excess	χ32	L_{dust}/L_* [a] ($\times10^{-5}$)
HD 870[b]	2.3 ± 0.4	0.009	0.8	< 12	2.2 ± 0.2	0.082	3.8	1.3
HD 1461[b]	4.0 ± 0.8	0.010	1.0	< 8.6	7.0 ± 1.0	0.162	5.1	1.8
HD 1581[c]	16.5 ± 1.2	0.005	0.5	< 8.3	2.0 ± 1.4	0.006	0.3	< 0.9
HD 3765	0.1 ± 0.5	0.000	0.0	< 14	−0.4 ± 0.4	−0.014	−0.6	< 1.5
HD 4308	0.0 ± 0.5	0.000	0.0	< 9.9	−0.2 ± 0.2	−0.004	−0.2	< 1.1
HD 4813[d]	2.6 ± 0.8	0.002	0.2	< 7.5	−0.5 ± 0.8	−0.004	−0.2	< 0.8
HD 5133	1.9 ± 0.7	0.004	0.4	< 15	0.5 ± 0.5	0.013	0.6	< 1.6
HD 7439	−7.0 ± 0.7	−0.009	−0.9	< 6.8	−0.7 ± 0.8	−0.007	−0.3	< 0.7
HD 8997	−4.0 ± 0.7	−0.014	−1.4	< 14	1.7 ± 0.3	0.054	2.5	< 1.5
HD 9407	1.8 ± 0.4	0.004	0.4	< 10	−0.6 ± 0.3	−0.017	−0.8	< 1.1
HD 10360[d,e]	−109.3 ± 2.2	−0.093	−8.9	< 12	2.2 ± 0.8	0.017	0.8	< 1.3
HD 10647[b]	2.0 ± 0.6	0.003	0.3	< 8.3	96.4 ± 2.8	1.204	21.7	13.0
HD 10780	−12.9 ± 0.7	−0.012	−1.2	< 12	−0.2 ± 0.9	−0.002	−0.1	< 1.3
HD 14412[c]	−0.6 ± 0.4	−0.001	−0.1	< 9.9	−0.5 ± 0.4	−0.008	−0.4	< 1.1
HD 16673	3.7 ± 0.5	0.007	0.7	< 7.1	2.5 ± 0.4	0.039	1.9	< 0.8
HD 16895[d]	8.8 ± 1.4	0.003	0.3	< 7.5	−6.9 ± 1.5	−0.028	−1.3	< 0.8
HD 18803	0.6 ± 0.4	0.002	0.1	< 11	−0.1 ± 0.7	−0.002	−0.1	< 1.2
HD 21197	−11.8 ± 0.5	−0.032	−3.2	< 19	0.5 ± 0.4	0.015	0.7	< 2.1
HD 21749	2.2 ± 0.4	0.008	0.8	< 16	0.9 ± 0.4	0.030	1.3	< 1.8
HD 23356	−3.9 ± 0.5	−0.009	−0.9	< 14	1.1 ± 0.2	0.023	1.1	< 1.5
HD 24451	3.8 ± 0.5	0.015	1.5	< 16	0.1 ± 0.3	0.003	0.1	< 1.8
HD 24916	2.6 ± 0.5	0.010	0.9	< 16	0.7 ± 0.2	0.022	1.0	< 1.8
HD 26491	1.8 ± 0.5	0.004	0.4	< 9.5	−0.5 ± 0.6	−0.011	−0.5	< 1.0
HD 27274	−0.2 ± 0.4	−0.001	−0.1	< 19	−0.1 ± 0.6	−0.003	−0.1	< 2.1
HD 28343[d]	6.9 ± 0.7	0.015	1.5	< 23	0.4 ± 0.5	0.010	0.4	< 2.5
HD 30501	−2.1 ± 0.4	−0.009	−0.9	< 13	0.7 ± 0.5	0.031	1.1	< 1.4
HD 30652[c]	−6.9 ± 5.0	−0.002	−0.2	< 7.1	−0.5 ± 3.4	−0.001	−0.1	< 0.8
HD 32147[d]	−13.5 ± 0.8	−0.011	−1.1	< 15	0.4 ± 0.7	0.003	0.1	< 1.6
HD 36003	−0.6 ± 0.5	−0.001	−0.1	< 19	−0.5 ± 0.3	−0.010	−0.5	< 2.1
HD 36395[d]	19.5 ± 1.1	0.016	1.5	< 30	−3.3 ± 1.0	−0.025	−1.2	< 3.2
HD 38230	−1.2 ± 0.5	−0.004	−0.4	< 12	−0.1 ± 0.3	−0.001	−0.1	< 1.3
HD 38392[d]	3.4 ± 0.7	0.003	0.3	< 14	0.4 ± 0.8	0.004	0.2	< 1.5
HD 38393	6.4 ± 2.1	0.001	0.1	< 7.5	4.5 ± 2.2	0.010	0.5	< 0.8
HD 38858[d]	−9.1 ± 0.6	−0.013	−1.3	< 9.7	13.4 ± 1.2	0.190	6.8	2.3
HD 40136[d]	23.1 ± 1.0	0.010	1.0	< 5.7	43.5 ± 2.3	0.163	7.3	1.2
HD 40307	2.9 ± 0.6	0.006	0.6	< 15	0.6 ± 0.4	0.011	0.5	< 1.6
HD 42807	1.9 ± 0.5	0.005	0.4	< 9.2	−0.9 ± 0.7	−0.021	−0.8	< 1.0
HD 43042	5.0 ± 0.7	0.006	0.6	< 7.1	−0.9 ± 0.6	−0.008	−0.4	< 0.8
HD 45184[b]	4.7 ± 0.4	0.012	1.2	< 9.2	16.3 ± 0.7	0.377	12.8	4.4
HD 46588[d]	8.6 ± 0.5	0.010	1.0	< 7.9	−0.9 ± 0.4	−0.010	−0.5	< 0.9
HD 49095	−2.0 ± 0.5	−0.004	−0.3	< 7.1	−0.2 ± 0.3	−0.004	−0.2	< 0.8
HD 50281[d]	−18.4 ± 0.5	−0.021	−2.0	< 15	2.7 ± 0.7	0.028	1.3	< 1.6
HD 50692[c]	−4.3 ± 0.5	−0.005	−0.5	< 8.6	−0.3 ± 0.5	−0.004	−0.2	< 0.9
HD 52711[c]	−0.4 ± 0.5	0.000	0.0	< 9.7	1.7 ± 0.4	0.027	1.3	< 1.0
HD 53705[d]	4.7 ± 0.7	0.004	0.4	< 9.5	−3.0 ± 0.6	−0.029	−1.4	< 1.0
HD 59468	4.5 ± 0.5	0.013	1.3	< 9.9	−0.1 ± 0.4	−0.003	−0.1	< 1.1
HD 62613[c]	1.2 ± 0.4	0.003	0.3	< 11	−0.9 ± 0.4	−0.019	−0.9	< 1.2
HD 65583	1.4 ± 0.4	0.004	0.4	< 11	0.3 ± 0.4	0.008	0.4	< 1.2
HD 65907	1.7 ± 0.6	0.003	0.3	< 8.6	2.5 ± 0.5	0.028	1.3	< 0.9
HD 67199	−2.0 ± 0.3	−0.006	−0.6	< 13	0.4 ± 0.3	0.012	0.5	< 1.4
HD 68017	−0.5 ± 0.5	−0.001	−0.1	< 9.7	−0.5 ± 0.6	−0.011	−0.4	< 1.0
HD 68146[d]	1.5 ± 0.4	0.002	0.2	< 7.5	−0.5 ± 0.4	−0.007	−0.3	< 0.8
HD 69897[c]	2.5 ± 0.7	0.003	0.3	< 7.1	−1.9 ± 0.7	−0.017	−0.8	< 0.8
HD 71148[c]	0.3 ± 0.5	0.001	0.1	< 9.9	0.1 ± 0.5	0.003	0.1	< 1.1
HD 71243[d]	−3.0 ± 1.3	−0.002	−0.2	< 6.8	−2.9 ± 1.8	−0.014	−0.6	< 0.7
HD 72673[d]	10.0 ± 0.6	0.014	1.4	< 12	−1.4 ± 0.6	−0.021	−1.0	< 1.3
HD 72760[f]	2.5 ± 0.5	0.009	0.9	< 9.9	−0.5 ± 0.3	−0.019	−0.8	< 1.1
HD 73667	−3.5 ± 0.4	−0.014	−1.3	< 13	−2.0 ± 0.3	−0.071	−3.1	< 1.4
HD 76653[d]	3.3 ± 0.5	0.006	0.6	< 7.1	11.6 ± 0.7	0.197	8.1	1.8
HD 78366[d]	−3.5 ± 0.5	−0.006	−0.6	< 8.3	−1.2 ± 0.8	−0.021	−0.9	< 0.9
HD 82106	0.9 ± 0.8	0.002	0.2	< 15	0.4 ± 0.8	0.008	0.3	< 1.6
HD 84035	1.9 ± 0.5	0.007	0.7	< 19	−0.5 ± 0.3	−0.017	−0.7	< 2.1
HD 85512[d]	8.8 ± 0.7	0.015	1.5	< 27	−1.0 ± 0.7	−0.014	−0.6	< 3.0
HD 90089[d]	−1.8 ± 0.6	−0.002	−0.2	< 6.0	1.2 ± 0.6	0.014	0.7	< 0.6

Table 4
(Continued)

Star	8.5–12 μm				30–34 μm			
	Excess (mJy)	Fractional Excess	$\chi 10$	$L_{\rm dust}/L_*$ [a] ($\times 10^{-5}$)	Excess (mJy)	Fractional Excess	$\chi 32$	$L_{\rm dust}/L_*$ [a] ($\times 10^{-5}$)
HD 90156	5.1 ± 0.4	0.018	1.7	< 9.9	0.2 ± 0.3	0.005	0.2	< 1.1
HD 91324[d]	21.6 ± 1.1	0.016	1.5	< 7.1	3.3 ± 0.6	0.022	1.1	< 0.8
HD 91889[g]	2.0 ± 0.4	0.003	0.3	< 7.5	−1.5 ± 0.8	−0.021	−0.9	< 0.8
HD 97101	0.5 ± 0.6	0.001	0.1	< 23	0.2 ± 0.3	0.005	0.2	< 2.5
HD 98281	−5.3 ± 0.3	−0.022	−2.1	< 11	−0.4 ± 0.4	−0.012	−0.5	< 1.2
HD 100180	1.4 ± 0.5	0.004	0.4	< 8.6	−1.5 ± 0.4	−0.034	−1.5	< 0.9
HD 100623[d]	1.9 ± 0.9	0.002	0.2	< 12	−3.1 ± 0.6	−0.030	−1.4	< 1.3
HD 102438[c]	6.6 ± 0.8	0.017	1.6	< 9.9	0.9 ± 0.4	0.020	0.9	< 1.1
HD 103932	−6.3 ± 0.9	−0.008	−0.7	< 19	−2.3 ± 0.5	−0.027	−1.3	< 2.1
HD 104067	−0.8 ± 0.5	−0.004	−0.4	< 14	−0.4 ± 0.3	−0.016	−0.7	< 1.5
HD 104731[c]	8.1 ± 0.6	0.009	0.9	< 7.1	−0.3 ± 0.6	−0.002	−0.1	< 0.8
HD 108954	2.7 ± 0.5	0.005	0.5	< 8.3	−0.8 ± 0.4	−0.017	−0.8	< 0.9
HD 109200	−0.9 ± 0.5	−0.002	−0.2	< 13	−0.2 ± 0.2	−0.006	−0.3	< 1.4
HD 109524	−1.3 ± 0.4	−0.004	−0.4	< 19	−0.5 ± 0.4	−0.013	−0.6	< 2.1
HD 110810	1.2 ± 0.4	0.004	0.4	< 15	0.6 ± 0.4	0.024	0.9	< 1.6
HD 110897[c]	−2.2 ± 0.5	−0.003	−0.3	< 8.6	4.0 ± 0.6	0.062	2.8	0.7
HD 111395[c]	−0.9 ± 0.5	−0.002	−0.2	< 11	0.5 ± 0.4	0.010	0.5	< 1.1
HD 113194	4.2 ± 0.6	0.012	1.1	< 19	0.1 ± 0.3	0.003	0.1	< 2.1
HD 114710[c]	33.1 ± 1.7	0.014	1.4	< 8.3	−3.7 ± 1.4	−0.015	−0.7	< 0.9
HD 115617[c,h]	−3.6 ± 1.4	−0.002	−0.2	< 9.9	30.8 ± 2.0	0.115	5.3	1.5
HD 117043[c,h]	−1.6 ± 0.5	−0.004	−0.4	< 10	3.2 ± 0.5	0.064	2.8	0.8
HD 120690[c]	−8.5 ± 0.6	−0.016	−1.6	< 9.9	1.3 ± 0.5	0.023	1.0	< 1.1
HD 121560	−9.5 ± 0.6	−0.021	−2.1	< 7.1	1.1 ± 0.5	0.023	1.0	< 0.8
HD 122064	5.9 ± 0.6	0.006	0.6	< 15	−1.7 ± 0.5	−0.018	−0.9	< 1.6
HD 124580	−0.2 ± 0.4	−0.001	−0.1	< 8.3	−0.5 ± 0.4	−0.013	−0.6	< 0.9
HD 126053	9.6 ± 0.6	0.017	1.7	< 9.0	0.0 ± 0.4	0.000	0.0	< 1.0
HD 128165	3.1 ± 0.8	0.007	0.7	< 15	0.4 ± 0.6	0.010	0.4	< 1.6
HD 128400[f]	5.1 ± 0.4	0.015	1.5	< 9.9	1.7 ± 0.6	0.047	1.7	< 1.1
HD 128987[f]	−0.3 ± 0.6	−0.002	−0.2	< 10	0.0 ± 0.5	0.001	0.0	< 1.1
HD 129502[d]	−12.9 ± 1.7	−0.005	−0.5	< 6.0	−1.7 ± 3.0	−0.006	−0.3	< 0.6
HD 130992	0.7 ± 0.4	0.003	0.3	< 15	−0.6 ± 0.3	−0.018	−0.8	< 1.6
HD 131977[d]	4.4 ± 1.2	0.002	0.2	< 16	7.1 ± 1.1	0.033	1.6	< 1.8
HD 132254[d]	7.1 ± 0.7	0.010	1.0	< 7.5	2.6 ± 0.7	0.035	1.6	< 0.8
HD 134060	−0.6 ± 0.5	−0.002	−0.1	< 9.2	0.2 ± 0.5	0.003	0.1	< 1.0
HD 134083[c]	9.4 ± 0.6	0.008	0.8	< 6.8	−1.9 ± 1.2	−0.016	−0.7	< 0.7
HD 135599[f]	1.7 ± 0.6	0.004	0.4	< 12	13.9 ± 0.7	0.323	11.0	5.1
HD 142709	0.0 ± 0.4	0.001	0.0	< 16	2.0 ± 0.4	0.060	2.5	< 1.8
HD 142860[c]	5.4 ± 2.5	0.001	0.1	< 7.1	0.9 ± 2.8	0.002	0.1	< 0.8
HD 144579	−0.7 ± 0.5	−0.001	−0.1	< 11	0.5 ± 0.4	0.009	0.4	< 1.2
HD 145825	1.2 ± 0.5	0.003	0.3	< 9.0	0.5 ± 0.3	0.013	0.6	< 1.0
HD 149661[c]	1.2 ± 0.7	0.001	0.1	< 14	−0.6 ± 1.0	−0.005	−0.2	< 1.5
HD 151288[d]	0.7 ± 0.8	0.003	0.3	< 19	−0.6 ± 0.3	−0.008	−0.4	< 2.1
HD 154345	−4.4 ± 0.5	−0.011	−1.1	< 11	−1.0 ± 0.4	−0.025	−1.2	< 1.2
HD 154363[d]	−5.5 ± 0.7	−0.010	−1.0	< 19	−0.1 ± 0.5	−0.001	0.0	< 2.1
HD 154577[b]	−4.8 ± 0.5	−0.013	−1.3	< 14	2.9 ± 0.3	0.079	3.5	1.4
HD 156026[d]	−1.0 ± 1.1	−0.001	−0.1	< 19	1.1 ± 0.9	0.006	0.3	< 2.1
HD 157214[c]	1.5 ± 0.4	0.001	0.1	< 8.6	−0.6 ± 0.8	−0.007	−0.3	< 0.9
HD 157347	−0.6 ± 0.5	−0.001	−0.1	< 9.9	−1.5 ± 0.4	−0.027	−1.3	< 1.1
HD 157881[d]	8.4 ± 0.7	0.009	0.9	< 19	−0.2 ± 0.7	−0.003	−0.1	< 2.1
HD 158633[d,h]	2.6 ± 0.6	0.004	0.4	< 12	6.6 ± 0.6	0.097	4.4	1.5
HD 160032[d]	−0.4 ± 0.7	−0.001	−0.1	< 6.2	4.5 ± 1.0	0.035	1.6	< 0.7
HD 162004[e]	−4.2 ± 0.4	−0.007	−0.7	< 8.6	2.0 ± 0.4	0.032	1.5	< 0.9
HD 164259[d]	11.7 ± 0.5	0.010	1.0	< 6.0	0.1 ± 0.9	0.000	0.0	< 0.6
HD 164922	−0.1 ± 0.6	0.000	0.0	< 12	0.2 ± 0.4	0.007	0.3	< 1.3
HD 165401	2.1 ± 0.5	0.007	0.6	< 8.6	−0.3 ± 0.4	−0.009	−0.4	< 0.9
HD 168009	0.8 ± 0.5	0.001	0.1	< 9.2	−1.4 ± 0.5	−0.027	−1.2	< 1.0
HD 170493	4.1 ± 0.3	0.017	1.6	< 15	−2.4 ± 0.5	−0.090	−3.3	< 1.6
HD 170657	5.8 ± 0.5	0.012	1.2	< 13	−4.8 ± 0.6	−0.097	−4.0	< 1.4
HD 172051[d]	−5.3 ± 0.6	−0.007	−0.7	< 9.9	4.1 ± 0.7	0.052	2.4	< 1.1
HD 177565[d]	−0.8 ± 0.6	−0.001	−0.1	< 9.9	0.3 ± 0.5	0.005	0.2	< 1.1
HD 182488[d]	−0.3 ± 0.5	0.000	0.0	< 11	−1.5 ± 0.4	−0.026	−1.2	< 1.2
HD 183870	4.9 ± 0.5	0.017	1.7	< 14	1.3 ± 0.4	0.044	1.9	< 1.5
HD 184385	4.8 ± 0.5	0.014	1.4	< 9.9	−3.6 ± 0.7	−0.099	−3.4	< 1.1
HD 185144[c,e,h]	−99.6 ± 2.6	−0.031	−3.1	< 12	5.1 ± 1.2	0.015	0.8	< 1.3

Table 4
(Continued)

Star	8.5–12 μm				30–34 μm			
	Excess (mJy)	Fractional Excess	$\chi 10$	L_{dust}/L_* [a] ($\times 10^{-5}$)	Excess (mJy)	Fractional Excess	$\chi 32$	L_{dust}/L_* [a] ($\times 10^{-5}$)
HD 189245[d]	−16.7 ± 0.5	−0.028	−2.8	< 7.5	−0.7 ± 0.5	−0.011	−0.5	< 0.8
HD 189567[c]	3.4 ± 0.4	0.006	0.5	< 9.5	2.1 ± 0.5	0.032	1.5	< 1.0
HD 190404	−8.5 ± 0.6	−0.023	−2.3	< 13	−1.1 ± 0.3	−0.028	−1.3	< 1.4
HD 190406[d,h]	4.8 ± 0.5	0.007	0.7	< 9.0	1.5 ± 0.3	0.021	1.0	< 1.0
HD 190470	5.0 ± 0.4	0.022	2.2	< 15	5.8 ± 0.2	0.248	10.5	4.8
HD 191785	1.3 ± 0.4	0.005	0.5	< 13	−0.3 ± 0.2	−0.010	−0.4	< 1.4
HD 191849[d]	6.9 ± 0.8	0.006	0.6	< 23	4.0 ± 0.8	0.037	1.7	< 2.5
HD 192310[d]	−6.0 ± 0.7	−0.005	−0.5	< 12	−0.3 ± 1.0	−0.002	−0.1	< 1.3
HD 193664[c]	1.7 ± 0.5	0.003	0.3	< 9.5	−0.6 ± 0.5	−0.010	−0.5	< 1.0
HD 197076	−7.4 ± 0.7	−0.018	−1.8	< 9.9	−1.5 ± 0.6	−0.038	−1.5	< 1.1
HD 197692[c]	−37.8 ± 2.0	−0.019	−1.9	< 6.8	1.7 ± 2.0	0.008	0.4	< 0.7
HD 199260[d,h]	−6.5 ± 0.7	−0.011	−1.1	< 7.5	8.0 ± 0.4	0.135	6.3	1.3
HD 205390	0.9 ± 0.5	0.002	0.2	< 14	0.3 ± 0.3	0.009	0.4	< 1.5
HD 205536	4.2 ± 0.3	0.014	1.4	< 11	1.9 ± 0.4	0.061	2.5	< 1.2
HD 210302[c]	0.1 ± 0.8	0.001	0.1	< 7.1	−1.0 ± 0.9	−0.008	−0.4	< 0.8
HD 210918[c]	4.1 ± 0.5	0.008	0.8	< 9.9	−1.1 ± 0.3	−0.021	−1.0	< 1.1
HD 212168	1.9 ± 0.5	0.004	0.4	< 9.5	3.3 ± 0.5	0.063	2.8	< 1.0
HD 213042	0.9 ± 0.4	0.003	0.3	< 19	0.2 ± 0.4	0.005	0.2	< 2.1
HD 213845[d]	4.4 ± 0.6	0.006	0.6	< 7.5	2.6 ± 0.5	0.033	1.6	< 0.8
HD 218511	0.0 ± 0.4	0.000	0.0	< 19	1.3 ± 0.4	0.039	1.7	< 2.1
HD 219623[d]	8.5 ± 0.5	0.012	1.2	< 7.5	13.8 ± 0.7	0.181	7.9	1.7
HD 221354	3.0 ± 0.5	0.007	0.7	< 14	3.1 ± 0.5	0.064	2.8	< 1.5
HD 222237[d,h]	−10.1 ± 0.6	−0.018	−1.8	< 16	0.0 ± 0.3	−0.001	−0.1	< 1.8
HD 222335	−4.1 ± 0.4	−0.012	−1.2	< 13	0.9 ± 0.3	0.026	1.2	< 1.4
Average[i]	...	...	...	11 ± 4	...	...	...	1.3 ± 0.5

Notes.
[a] Limits on L_{dust}/L_* from using Equation (1) and three times the dispersion in the fractional excess of the whole population.
[b] Star has public MIPS 24 and 70 μm data that was reduced as described in Section 3.2.
[c] Star has MIPS 24 and 70 μm data from the FGK survey (Beichman et al. 2006a).
[d] Star has MIPS 24 and 70 μm data from the SIM/TPF survey (Beichman et al. 2006b).
[e] Data has significant pointing errors or a close companion so IRS data may not be accurate.
[f] Star has MIPS 24 and 70 μm data from Plavchan et al. (2009).
[g] Star has MIPS 24 and 70 μm data from Trilling et al. (2008).
[h] IRS data has been co-added with IRS data from the FGK or SIM/TPF program (see Table 3).
[i] Average values of L_{dust}/L_* (3σ limits or detections) after 2σ rejection of outliers.

when compared to the dispersion in the overall population. To assess the significance of any possible excess, we define $\chi 10$ and $\chi 32$ as $[F_\nu(\text{Observed}) - F_\nu(\text{Photosphere})]/\text{Noise}$ for the two photometric bands, where Noise is a combination of the dispersion in the fractional excess of the individual spectrum and the population-averaged dispersion: 1% (8.5–12 μm) and 2% (30–34 μm). For a star to have an excess, we require $\chi > 3$ for an IRS-only detection or $\chi > 2$ if the star also has a MIPS 70 μm excess. Based on the data presented in Table 4, we can claim statistically significant 30–34 μm excesses for 16 stars (Table 5). By this same criterion, no stars in the sample have a significant 8.5–12 μm excess.

Complete IRS data for all 16 stars with excesses in these wavelengths are presented in the appendix. Figure 8 shows the IRS spectra for four representative stars without excesses, while Figure 9 shows the IRS spectra for all stars that do have significant excesses in the IRS wavelengths. The dotted lines in the right-hand panels of Figures 8 and 9 show an estimate of the 2σ dispersion in the deviations from the photospheric models based on the entire sample; deviations between these lines should be regarded with skepticism.

4.1. Statistics of Detections

We detected IRS excess emission toward 16 stars. These excesses begin longward of ~25 μm for 10 stars, and between ~15 and 25 μm for the other six stars. Two of the excess detections are of borderline significance and are included because of the additional information of a MIPS 70 μm excess (see Section 4.2): HD 110897 and HD 117043, both with $\chi 32 = 2.8$. Out of the sample of 152 stars, these 16 stars correspond to a 30–34 μm excess detection rate of 10.5% ± 2.6%, which is consistent with the fraction of stars with excesses found in a previous IRS survey: 12% ± 5% (Beichman et al. 2006a). We must, however, correct these statistics for the sources that were not observed as part of this sample because they were claimed as part of other, earlier *Spitzer* programs. Comparing our initial selection of sources meeting our astrophysical criteria with early guaranteed time or legacy programs yields 51 additional stars, which we list in Table 6. With this correction, the success rate for long-wavelength IRS excesses is not 16/152 = 10.5% ± 2.6%, but 24/203 = 11.8% ± 2.4%, essentially the same as found in our earlier determination (Beichman et al. 2006a), but with much lower uncertainty.

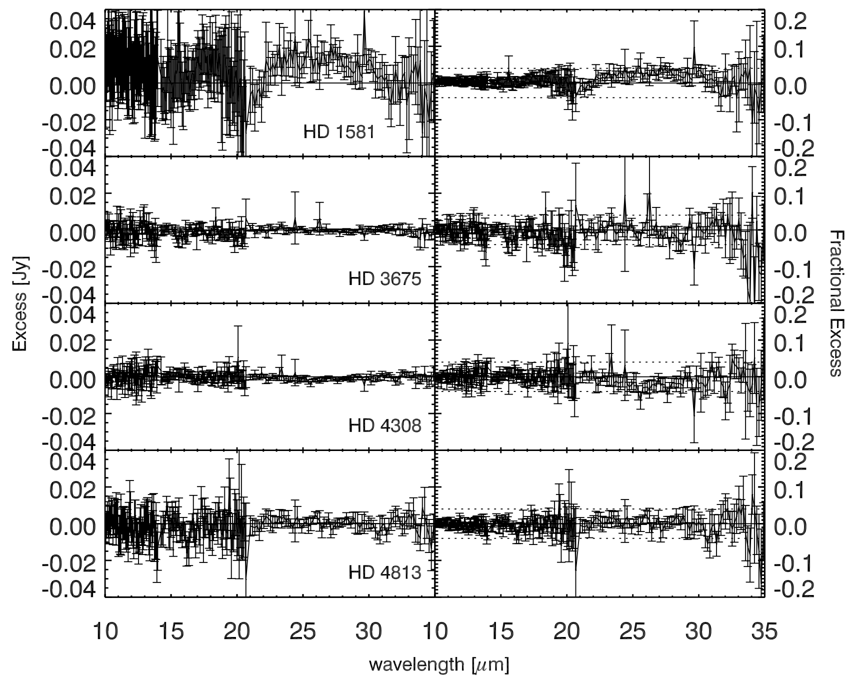

Figure 8. IRS spectra for four stars with no excesses. The left-hand plots show the excess in Jy relative to the photosphere after normalization with respect to the first 10 points of each module. The right-hand plots show the fractional amount of the excess relative to the photosphere after normalization. The dotted lines in the right panels show an estimate of the 2σ dispersion in the deviations from the photospheric models. None of these stars have fractional excesses outside of these 2σ limits.

Table 5
Stars with IRS and/or MIPS Excesses

Star	IRS 30–34 μm			MIPS 70 μm					MIPS Data Source[a]
	Fractional Excess	χ32	Excess?	F_ν (mJy)	Excess (mJy)	Fractional Excess	χ70	Excess?	
HD 870	0.08	3.8	Yes	21 ± 4	15	2.6	3.9	Yes	This paper[b]
HD 1461	0.16	5.1	Yes	61 ± 6	52	5.7	8.6	Yes	This paper[b]
HD 10647	1.20	21.7	Yes	878 ± 8[c]	862	52.1	94.1	Yes	G. Bryden et al. (2009, in preparation)
HD 38858	0.19	6.8	Yes	190 ± 9[c]	175	11.7	17.2	Yes	G. Bryden et al. (2009, in preparation)
HD 40136	0.16	7.3	Yes	95 ± 5	39	0.7	6.4	Yes	Beichman et al. (2006b)
HD 45184	0.38	12.8	Yes	119 ± 7	110	12.1	15.9	Yes	This paper[b]
HD 76653	0.20	8.1	Yes	38 ± 11	26	2.1	4.3	Yes	Beichman et al. (2006b)
HD 90089	0.01	0.7	No	41 ± 3	24	1.5	8.3	Yes	Beichman et al. (2006b)
HD 110897	0.06	2.8	Weak	56 ± 4	42	3.1	11.0	Yes	Trilling et al. (2008)
HD 115617	0.15	5.3	Yes	224 ± 8[c]	179	3.0	15.7	Yes	G. Bryden et al. (2009, in preparation)
HD 117043	0.11	2.8	Weak	15 ± 3	7	0.8	1.9	Weak	Bryden et al. (2006)
HD 132254	0.03	1.6	No	25 ± 3	10	0.7	3.5	Yes	Beichman et al. (2006b)
HD 135599	0.32	11.0	Yes	101 ± 5	92	10.0	18.4	Yes	Plavchan et al. (2009)
HD 154577	0.08	3.5	Yes	14 ± 7	6	0.8	0.9	No	This paper[d]
HD 158633	0.11	4.4	Yes	59 ± 3	45	3.1	13.5	Yes	Beichman et al. (2006b)
HD 160032	0.04	1.6	No	44 ± 5	17	0.7	3.2	Yes	Beichman et al. (2006b)
HD 190470	0.25	10.5	Yes	79 ± 60	74	15.6	1.2	No[e]	This paper[d]
HD 199260	0.14	6.3	Yes	47 ± 4	34	2.8	8.4	Yes	Beichman et al. (2006b)
HD 219623	0.18	7.9	Yes	50 ± 3	34	2.2	10.1	Yes	Beichman et al. (2006b)

Notes. There are 60 additional stars with MIPS data, but no excesses. These are noted in Table 4.
[a] MIPS data were reduced as described in Section 3.2.
[b] Data from *Spitzer* GO Program 30490, PI: D. Koerner.
[c] Flux from a model fit to the resolved disk, not aperture photometry.
[d] Data from *Spitzer* GTO Program 50150, PI: G. Rieke.
[e] This star is located in a particularly noisy field, so this cannot be considered an excess.

HD 72905 from the FGK survey (Beichman et al. 2006a) presents an interesting example of the challenges in identifying a weak infrared excess, particularly around 8–14 μm where the stellar photosphere is bright. Using IRAC data from the FEPS program (Carpenter et al. 2008), we use our standard technique to fit *Hipparcos* visible photometry, partially saturated 2MASS observations at JHK_s, and IRAC 3.6 and 4.8 μm data to a Kurucz model for a 6000 K G0V star with [Fe/H] = -0.08. The resultant fit has a reduced χ^2 of 0.97. Pinning the SL2 data to a Kurucz photosphere using the 20 shortest wavelength SL2 points requires a $\sim$2% adjustment to the SSC pipeline data and reveals *no fractional excess* from 5 to 8 μm greater than 2%. A

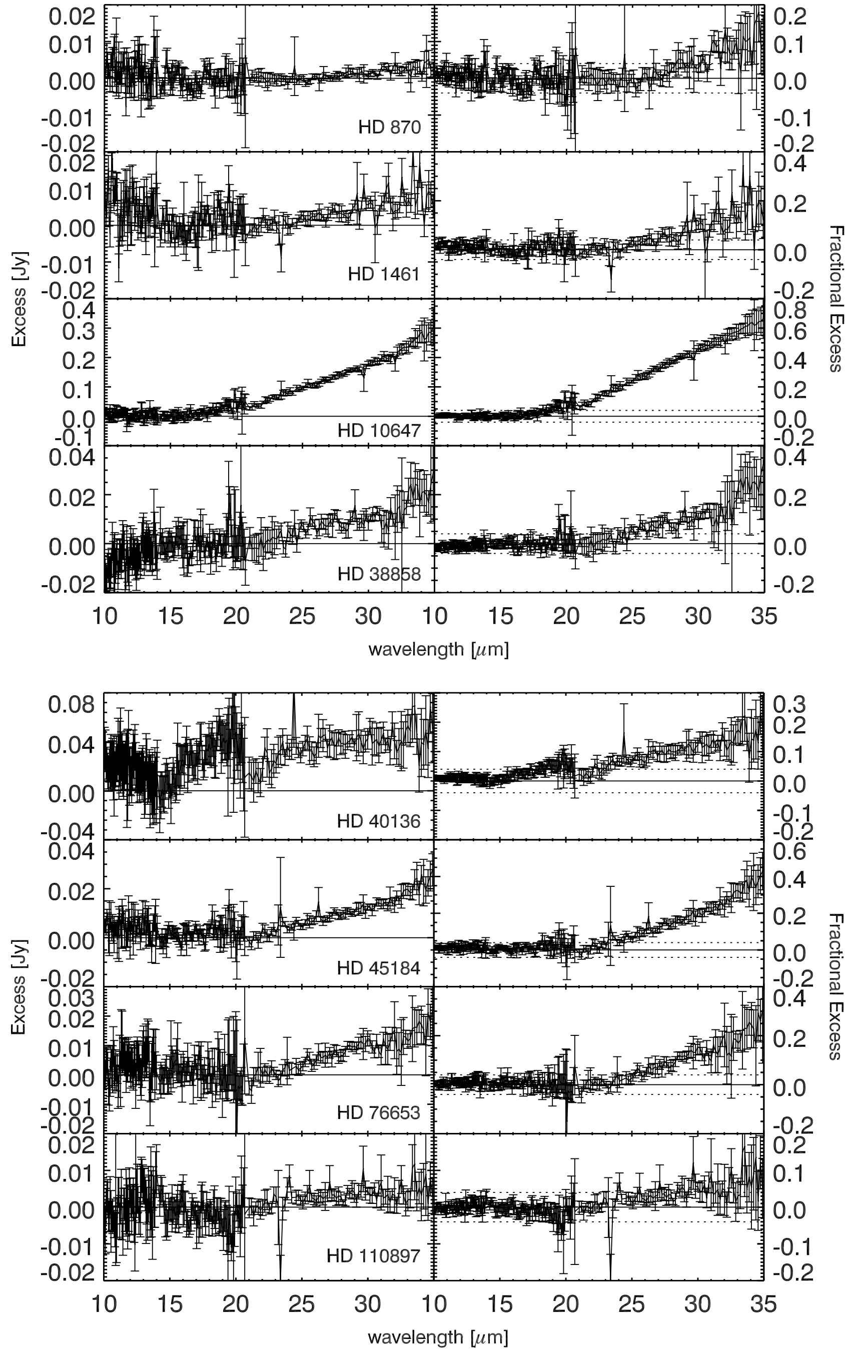

Figure 9. IRS spectra for stars with significant excesses. The left-hand plots show the excess in Jy relative to the photosphere after normalization with respect to the first 10 points of each module. The right-hand plots show the fractional amount of the excess relative to the photosphere after normalization. The dotted lines in the right panels show an estimate of the 2σ dispersion in the deviations from the photospheric models. All of these stars have fractional excesses that extend well above the 2σ threshold at longer wavelengths, and are significant at the 3σ level in the 30–34 μm band.

similar conclusion applies if we fit a solar photosphere (Rieke et al. 2008) to the IRAC 3.6 and 4.8 μm data. Extending the Kurucz photosphere to longer wavelengths yields a marginal excess of about 5% at IRAC 7.8 μm that carries through to IRS SL1 and MIPS 24 μm. The fractional excess has a significance at the $\sim 2\sigma$ level relative to the $\sim$2% uncertainties in the photospheric models. However, changing photospheric models makes the excess all but vanish. Fitting the Rieke et al. (2008) solar photosphere instead of the Kurucz model reduces the level of excess to 2% or less out to 25 μm (including MIPS 24). We conclude that we cannot claim any statistically significant excess at <25 μm. At longer wavelengths, the difference between photospheric models becomes less important, and the existence of a weak excess starting at $\lambda > 25$ μm becomes evident.

None of our sample stars showed excesses in the short-wavelength 8.5–12 μm portion of the spectrum, giving a fractional incidence of <0.7% for these mature stars. Adding in stars with previous *Spitzer* observations, we find an overall excess detection rate of 2 stars (HD 69830 and HD 109085) out of 203 = 1.0%±0.7% for the 8.5–12 μm band. This confirms the rarity of detectable short-wavelength excesses compared with

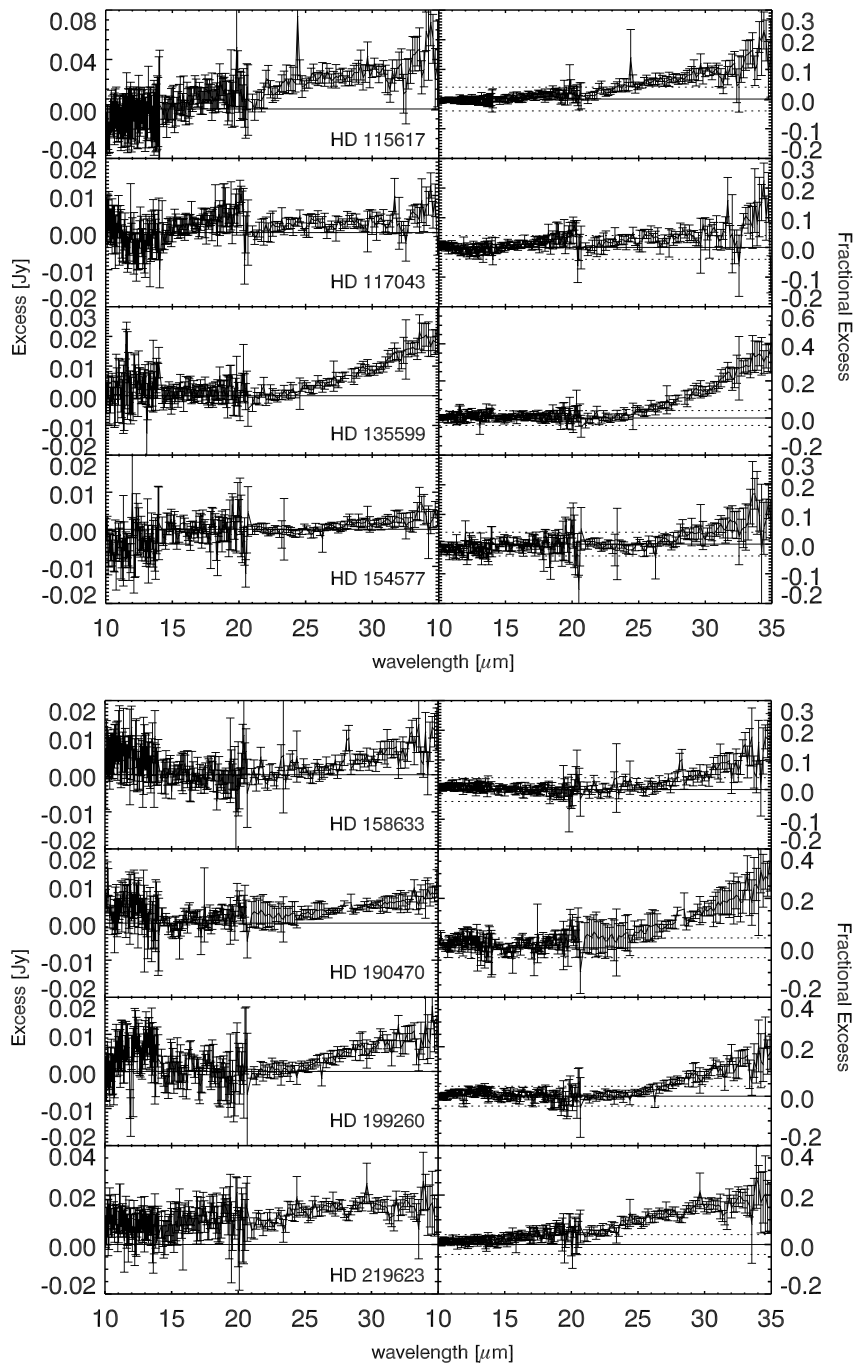

Figure 9. (Continued)

ones at longer wavelengths, as seen in Beichman et al. (2006a) and noted in earlier studies using the *Infrared Astronomical Satellite* (*IRAS*) and the *Infrared Space Observatory* (*ISO*).

The FEPS survey (Carpenter et al. 2008; Hillenbrand et al. 2008) used *Spitzer* to observe nearby sun-like stars with ages between 3 Myr and 3 Gyr. Using our criteria of $>3\sigma$ above the photosphere (or $>2\sigma$ with a known 70 μm excess), Hillenbrand et al. (2008) find excesses in the 30–34 μm band for 22 out of the sample of 328 stars, although not all stars in the sample have reported IRS spectra. Carpenter et al. (2008) measure excesses using colors rather than comparison with Kurucz models, and find 71 out of 314 stars (22.6% $\pm$ 2.7%) with excesses in the long-wavelength IRS band, and 2 out of 314 (0.6% $\pm$ 0.5%) in the short-wavelength IRS band. As these stars are on average younger than the stars in our sample, it is not surprising that there is a higher incidence of IRS-detected excesses.

Five stars in the sample were known to have planets as of May 2009: HD 4308 (Udry et al. 2006), HD 10647 (Mayor et al. 2003), HD 40307 (Mayor et al. 2009), HD 154345 (Wright et al. 2008), and HD 164922 (Butler et al. 2006). Of these five stars, only HD 10647 shows an excess at both 70 μm and IRS wavelengths. The other four planet-bearing systems have no detected excesses.

Table 6
Stars with Previous IRS Observations

Star	IRS Data			MIPS Data		
	8.5–12 μm Excess?	30–34 μm Excess?	IRS Data Source:	24 μm Excess?	70 μm Excess?	MIPS Data Source:
HD 7570	No	Yes	Beichman et al. (2006a)	Weak	Weak	Bryden et al. (2006)
HD 69830	Yes	Yes	Beichman et al. (2006a)	Yes	Weak	Bryden et al. (2006)
HD 72905	Weak	Yes	Beichman et al. (2006a)	Weak	Yes	Bryden et al. (2006)
HD 76151	No	Yes	Beichman et al. (2006a)	No	Yes	Bryden et al. (2006)
HD 109085	Yes	Yes	Examination of archive data[b], Chen et al. (2006)	Yes	Yes	Beichman et al. (2006b)
HD 128311	No	No	Beichman et al. (2006a)	No	Yes	Beichman et al. (2005a)
HD 151044	No	Yes	Examination of archive data[c]	Weak	Yes	This paper[a,c]
HD 206860	No	Yes	Beichman et al. (2006a)	No	Yes	Bryden et al. (2006)
HD 207129	No	Yes	Examination of archive data[d]	No	Yes	Trilling et al. (2008)
HD 693	No	No	Beichman et al. (2006a)	No	No	Beichman et al. (2006a)
HD 4628	No	No	Beichman et al. (2006a)	No	No	Bryden et al. (2006)
HD 7661	No	No	Examination of archive data[e]	No	No	Hillenbrand et al. (2008)
HD 9826	No	No	Beichman et al. (2006a)	No	No	Beichman et al. (2006a)
HD 29231	No	No	Examination of archive data[e]	No	No	Hillenbrand et al. (2008)
HD 33564	No	No	Examination of archive data[b], Chen et al. (2006)	No	No	Trilling et al. (2008)
HD 37572	No	No	Examination of archive data[e]	No	No	Hillenbrand et al. (2008)
HD 39091	No	No	Beichman et al. (2006a)	No	No	Beichman et al. (2005a)
HD 43834	No	No	Beichman et al. (2006a)	No	No	Bryden et al. (2006)
HD 44594	No	No	Examination of archive data[e]	No	No	Hillenbrand et al. (2008)
HD 55575	No	No	Beichman et al. (2006a)	No	No	Bryden et al. (2006)
HD 58855	No	No	Beichman et al. (2006a)	No	No	Bryden et al. (2006)
HD 75302	No	No	Examination of archive data[e]	No	No	Hillenbrand et al. (2008)
HD 75732	No	No	Beichman et al. (2006a)	No	No	Beichman et al. (2005a)
HD 84737	No	No	Beichman et al. (2006a)	No	No	Bryden et al. (2006)
HD 86728	No	No	Beichman et al. (2006a)	No	No	This paper[a,f]
HD 88742	No	No	Examination of archive data[e]	No	No	Hillenbrand et al. (2008)
HD 95128	No	No	Beichman et al. (2006a)	No	No	Beichman et al. (2005a)
HD 101501	No	No	Beichman et al. (2006a)	No	No	Bryden et al. (2006)
HD 105631	No	No	Examination of archive data[e]	No	No	Hillenbrand et al. (2008)
HD 115043	No	No	Examination of archive data[e]	No	No	Hillenbrand et al. (2008)
HD 120136	No	No	Beichman et al. (2006a)	No	No	Beichman et al. (2005a)
HD 142373	No	No	Beichman et al. (2006a)	No	No	Bryden et al. (2006)
HD 146233	No	No	Beichman et al. (2006a)	No	No	Bryden et al. (2006)
HD 154088	No	No	Beichman et al. (2006a)	No	No	Beichman et al. (2006a)
HD 154417	No	No	Examination of archive data[e]	No	No	Hillenbrand et al. (2008)
HD 159222	No	No	Examination of archive data[e]	No	No	Hillenbrand et al. (2008)
HD 166620	No	No	Beichman et al. (2006a)	No	No	Bryden et al. (2006)
HD 168151	No	No	Beichman et al. (2006a)	No	No	Bryden et al. (2006)
HD 173667	No	No	Beichman et al. (2006a)	No	No	Bryden et al. (2006)
HD 181321	No	No	Beichman et al. (2006a)	No	No	Bryden et al. (2006)
HD 185144	No	No	Beichman et al. (2006a)	No	No	Bryden et al. (2006)
HD 188376	No	No	Beichman et al. (2006a)	No	No	Bryden et al. (2006)
HD 191408	No	No	Beichman et al. (2006a)	No	No	Beichman et al. (2006a)
HD 196378	No	No	Beichman et al. (2006a)	No	No	Bryden et al. (2006)
HD 203608	No	No	Beichman et al. (2006a)	No	No	Bryden et al. (2006)
HD 205905	No	No	Examination of archive data[e]	No	No	Hillenbrand et al. (2008)
HD 206374	No	No	Examination of archive data[e]	No	No	Hillenbrand et al. (2008)
HD 217813	No	No	Beichman et al. (2006a)	No	No	Beichman et al. (2006a)
HD 212330	No	No	Beichman et al. (2006a)	No	No	Beichman et al. (2006a)
HD 217014	No	No	Beichman et al. (2006a)	No	No	Beichman et al. (2006a)
HD 222368	No	No	Beichman et al. (2006a)	No	No	Beichman et al. (2006a)

Notes.
[a] Public MIPS 24 and 70 μm data were reduced as described in Section 3.2.
[b] Data from *Spitzer* GTO Program 2, PI: J. Houck.
[c] Data from *Spitzer* GO Program 3401, PI: P. Abraham.
[d] Data from *Spitzer* GO Program 20065, PI: G. Bryden.
[e] Data from *Spitzer* Legacy Program 148, PI: M. Meyer.
[f] Data from *Spitzer* GO Program 30490, PI: D. Koerner.

4.2. Discussion of MIPS Results

We have MIPS data from other programs for about half (78) of the sample stars, as noted in Table 4. Table 5 lists all of the stars in our sample with IRS and/or MIPS 70 μm excesses. Of the 16 stars with IRS excesses, 14 have excesses in both the 30–34 μm IRS band and the MIPS photometry at 70 μm; only HD 154577 has an IRS excess with no detectable MIPS excess (HD 190470 is in a particularly noisy field close to the galactic plane, so the error bars on the 70 μm flux are so large that nothing can be said about whether or not there is an excess). Including the stars with previous IRS observations (Table 6) gives 22 stars with IRS excesses, 20 of which also have strong or weak MIPS 70 μm excesses. HD 110897 was not originally considered to have an IRS excess because of a marginal $\chi 32$ value (2.8), but this can be considered a weak excess because of the additional information of a strong MIPS 70 μm excess. HD 117043 has a marginally significant IRS excess ($\chi 32 = 2.8$) and a marginally significant MIPS 70 μm excess ($\chi 70 = 1.9$), but because $\chi 32$ is close to 3, this star was also included as a weak excess detection at both wavelengths.

Out of the 78 stars with both MIPS 70 μm and IRS data, only three stars (HD 90089, HD 132254, and HD 160032) have excess MIPS 70 μm emission with no significant IRS excess. Hillenbrand et al. (2008) find a similar trend, with >80% of their stars with MIPS 70 μm excesses also possessing IRS 33 μm excesses, and no reported stars possessing an IRS excess with no corresponding MIPS 70 μm excess. This implies that there may be a lower limit to debris disk temperatures, with a corresponding upper limit on disk sizes. Kuiper Belt analogs appear to happen preferentially in regions with temperatures around 50 K, and not at lower temperatures.

All of the stars with MIPS 70 μm data also have MIPS 24 μm measurements. Only two stars have greater than 2σ 24 μm fractional excesses: HD 10647 has a 24 μm excess that agrees with its large IRS excess. HD 38392 has a large apparent 24 μm excess with no IRS excess. However, examination of the 2MASS and MIPS 24 μm image for this star shows a bright companion star, HD 38393 ($K_s \sim 2.5$ mag), about 1$'$.5 away. Although the IRS slit does not cross the companion star, and therefore should not effect the spectrum, the uncertainty in the 24 μm photometry is inflated by the companion. Further, this star appears to be variable at the 5% level in a number of visible compilations (*Hipparcos* time series photometry and Nitschelm et al. 2000). An alternate explanation is the presence of an M dwarf companion. Such a companion could produce a 20% excess at 24 μm, and would be too faint to notice if the system's spectral type was measured using optical observations. Follow-up imaging using adaptive optics would be needed to test this hypothesis. Reinforcing the peculiarity of the MIPS 24 μm data point, the MIPS data do not show any 70 μm excess for HD 38392.

4.3. Limits on the Fractional Disk Luminosity

A useful metric for the limits on dust surrounding these stars is $L_{\rm dust}/L_\star$, which is related to the fractional flux limit of an excess relative to the Rayleigh–Jeans tail of the star's photosphere (Bryden et al. 2006; Beichman et al. 2006a):

$$\frac{L_{\rm dust}}{L_*} = \frac{F_{\rm dust}}{F_*}\frac{e^{x_d}-1}{x_d}\left(\frac{T_d}{T_*}\right)^3, \tag{1}$$

where $F_{\rm dust} = F_\nu(\text{Observed}) - F_\nu(\text{Photosphere})$. At the peak of the blackbody curve, $x_d \equiv h\nu/kT_d$ has a constant value

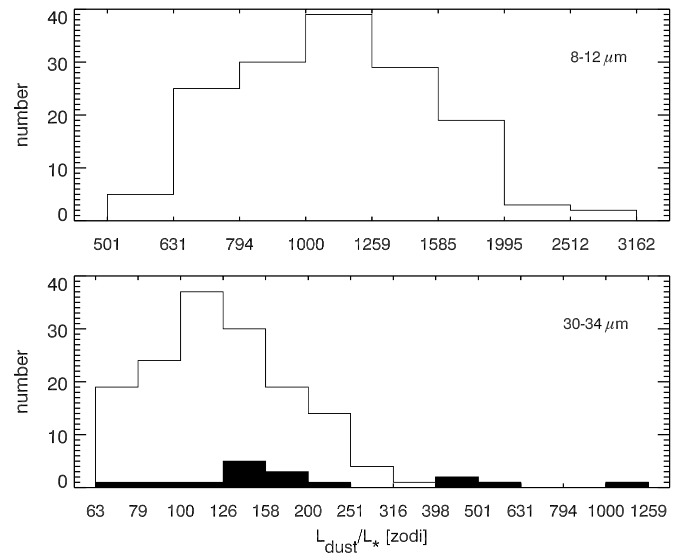

Figure 10. Calculated values of $L_{\rm dust}/L_\star$ for all sample stars in zodi (the value of $L_{\rm dust}/L_\star$ in our solar system: $\sim 10^{-7}$), using the 8.5–12 μm photometric band in the upper panel and using the 30–34 μm photometric band in the lower panel. All of the 8.5–12 μm measurements are upper limits based on $3\sigma_{\rm pop}$, as are most at 30–34 μm; the 16 stars with significant excesses at 30–34 μm (filled bars) have $L_{\rm dust}/L_\star$ calculated using Equation (1).

of 3.91, corresponding to $T_d = 367$ K at 10 μm. At this wavelength, $L_{\rm dust}/L_\star = 3.5 \times 10^{-3}\,(T_*/5600\,{\rm K})^{-3}\,F_{\rm dust}/F_\star$. At 30–34 μm, the corresponding equation is $L_{\rm dust}/L_\star = 1.3 \times 10^{-4}\,(T_*/5600\,{\rm K})^{-3}\,F_{\rm dust}/F_\star$, assuming $T_d = 115$ K. (For comparison, the typical dust temperatures traced by the MIPS 24 and 70 μm data are 154 and 53 K, respectively.) In Table 4 and Figure 10, we evaluate $L_{\rm dust}/L_\star$ for each star using the appropriate effective temperature (listed in Table 1), luminosity (from our stellar photosphere models), and its measured fractional excess in each band, $F_{\rm dust}/F_*$, or, in the case of an upper limit, $3\sigma_{\rm pop}$ where $\sigma_{\rm pop}$ is the dispersion in fractional excess averaged over the whole sample (0.010 at 8.5–12 μm; 0.028 at 30–34 μm). This definition of $L_{\rm dust}/L_\star$ assumes that the emitting material is all at the location where the peak of the T_d blackbody matches the wavelength of observation such that for stars with excesses the given value of $L_{\rm dust}/L_\star$ is actually a minimum. More dust emission, and higher values of $L_{\rm dust}/L_\star$, would be required for material located substantially interior or exterior to this point.

The 3σ limits on $L_{\rm dust}/L_\star$ at 8.5–12 μm and 30–34 μm have 2σ clipped average values of $L_{\rm dust}/L_\star = 11 \pm 4 \times 10^{-5}$ and $1.31 \pm 0.49 \times 10^{-5}$, respectively (Table 4). In comparison with our solar system, which has $L_{\rm dust}/L_\star \sim 10^{-7}$ (Backman & Paresce 1993; Dermott et al. 2002), the IRS results set limits (3σ) on warm (360 K) dust peaking at 10 μm of $\sim$1000 times the level of dust emission in our solar system. For cooler dust ($\sim$115 K) peaking at 30–34 μm, the 3σ limit corresponds to $\sim$100 times the nominal $L_{\rm dust}/L_\star$ of our zodiacal cloud. For objects with excesses in the IRS bands, we determine $L_{\rm dust}/L_\star$ explicitly by integrating over the data between 10 and 34 μm and using the models discussed below (Section 5.2.1) to extrapolate out to and beyond the MIPS 70 μm data point.

4.4. Comparing IRS and MIPS Statistics

Figure 11 summarizes the rates of IR excess detection in IRS spectral surveys and compares them with MIPS photometric results. For two wavelengths in each instrument, the distribution

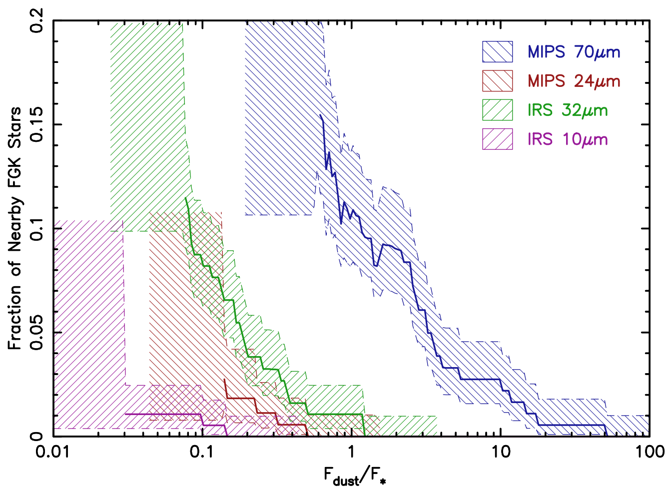

Figure 11. *Spitzer* detection rates of IR excess as a function of the fractional dust flux, $F_{\rm dust}/F_{\star}$. The various *Spitzer* instruments/wavelengths considered here are indicated in the figure legend. For MIPS photometry, 182 stars with spectral types F5–K5 are observed at 24 and 70 μm (Bryden et al. 2006; Beichman et al. 2006b; Trilling et al. 2008). For IRS spectra, 203 stars with spectral types F0–M0 are observed from 10 through 32 μm (from this survey and the stars in Table 6). Uncertainties in the underlying distribution due to small number statistics (shaded regions) are large below the detection limits of each instrument/wavelength.

(A color version of this figure is available in the online journal.)

of detection rates is shown as a function of the fractional dust flux ($F_{\rm dust}/F_{\star}$). Note that $F_{\rm dust}/F_{\star}$ can be easily translated to a fractional disk luminosity using Equation (1). It is clear from this figure that the dominant dust around solar-type stars tends to be colder than is optimal for detection at IRS wavelengths and generally exhibits higher $F_{\rm dust}/F_{\star}$ at longer wavelengths. Nevertheless, because we can detect excesses down to much smaller levels of $F_{\rm dust}/F_{\star}$ within the IRS spectra, the overall detection rate of IR excess for IRS at 32 μm is similar to that for MIPS at 70 μm. By comparison, IRS at 10 μm and MIPS at 24 μm have relatively few detections, but are both consistent with the overall trend from the other wavelengths. While it is difficult to extrapolate these distributions down to fainter values, the curves can be fit by log-normal distributions with median values of $F_{\rm dust}/F_{\star} \sim 0.06$ at 70 μm and $F_{\rm dust}/F_{\star} \sim 0.003$ at 32 μm. These fractional fluxes correspond to $L_{\rm dust}/L_{\star} \sim 5 \times 10^{-7}$ for a solar temperature star, consistent with estimates for our Kuiper Belt's emission (Stern 1996).

While the individual spectra provide the best measure of the range of dust temperatures in each system (Section 5.1), Figure 11 provides a sense of the generalized disk characteristics. The separation between the 32 μm and 70 μm distributions in Figure 11, for example, can be translated to a representative dust temperature of ∼65 K. In reality, a range of temperatures are present and, as is found in Section 5.2.1, the dust in each system is often not well fit by a single emission temperature, but rather by a distribution. This is also apparent from the overall statistics, as evidenced by the inability of a single blackbody to fit the trends seen in Figure 11; the separation between the 24 and 70 μm curves is consistent with 75 K dust, while the separation between the 10 and 70 μm curves corresponds to dust temperatures >100 K. A similar trend is found by Hillenbrand et al. (2008), who find that >1/3 of their surveyed debris disks have evidence for multiple dust temperatures based on their colors at MIPS and IRS wavelengths.

5. DISCUSSION

5.1. *Characteristics of the Spectra*

The excesses found in this survey are in most cases weak and relatively featureless beyond a simple rise to longer wavelengths. A few objects are exceptional: HD 10647 stands out for having a very strong excess, $L_{\rm dust}/L_{\star} = 10^{-3.9}$ rising up to 70 μm and continuing out to 160 μm (Tanner et al. 2009); this source also appears to be extended at 70 μm (G. Bryden et al., in preparation). HD 40136 and possibly HD 10647 show a bump around 20 μm which might be attributable to small grains. In addition to HD 10647, HD 38858 and HD 115617 both also show evidence for extended MIPS emission (G. Bryden et al. 2009, in preparation).

5.2. *Models for the Dust Excesses*

The IRS and MIPS excesses detected toward some of the 152 stars discussed here can be used to characterize the properties and spatial location of the emitting material. Unfortunately, even the simplest characterization cannot be unique given the wide variety of grain sizes and compositions as well as possible locations for these different species. The complexity of debris disks is evident as one attempts to model the most prominent debris disks for which high-quality IRS spectra and fully resolved maps are available (e.g., Vega; Su et al. 2005). In this section, we first apply a simple, single-component model that fits the majority of sources; we assume that uniform, large-grained (∼10 μm) dust is located in an annulus centered on the star. We then examine somewhat more sophisticated models for disks where additional complexity seems warranted.

5.2.1. *Simple Dust Models*

As a first step in analyzing these data, we fitted the IRS spectra and MIPS 70 μm photometry using a simple model of optically thin dust located within a single dust annulus centered around the star. As described in Beichman et al. (2006a), we calculated the power-law temperature profiles, $T(r) = T_0(L/L_{\odot})^{\alpha}(r/r_0)^{\beta}$, for grains in radiative equilibrium with the central star. We use dust emissivities for 10 μm silicate grains (Draine & Lee 1984; Weingartner & Draine 2001), the minimal size suggested by the lack of significant features in most of the spectra. For the 10 μm silicate grains, we obtained the following numerical relationship: $T(r) = 255\,K(L/L_{\odot})^{0.26}(r/{\rm AU})^{-0.49}$. These calculated coefficients and power-law constants closely follow analytical results (Backman & Paresce 1993). We then calculated the dust excess by integrating over the surface brightness of a disk between R_1 and R_2, with $F_{\nu}(\lambda) = \frac{2\pi}{D^2}\int \tau_0(\lambda)(r/r_0)^{-p}B_{\nu}(T(r))r\,dr$. The disk surface density distribution expected for grains dominated by Poynting–Robertson drag is roughly uniform with radius, i.e., $p = 0$ (Burns et al. 1979; Buitrago & Mediavilla 1985; Backman 2004). We examined a number of other cases with $0 < p < 1$ that would reflect different dust dynamics, but did not find results that were substantially different from those for $p = 0$.

We fitted the excess emission from a single annulus to 83 data points longward of 21 μm (just longward of the last point used for flux normalization of the LL1 IRS module) for 10 stars, and to 160 data points longward of 14 μm (just longward of the last point used for the flux normalization of the LL2 IRS module) for nine stars, depending on whether there was any hint of an excess shortward of 21 μm. We included the MIPS 70 μm data, which were available for all 19 of the stars modeled. By varying τ_0,

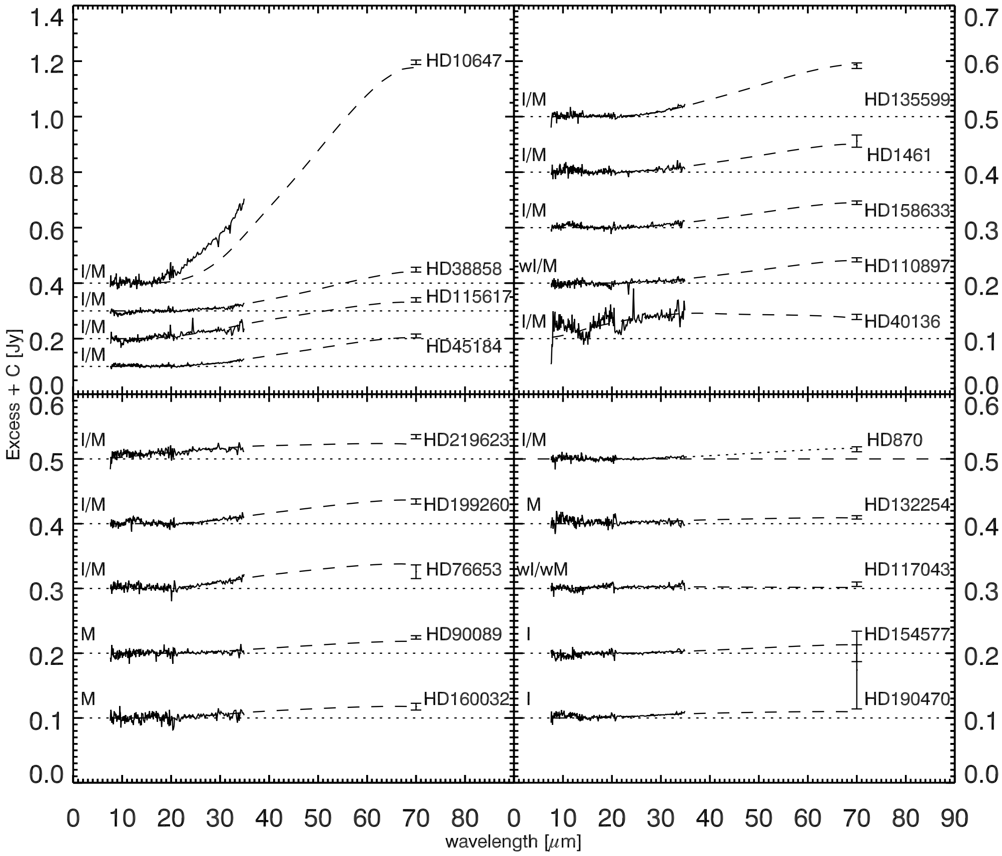

Figure 12. Measured and modeled spectra (using the simple model, see Section 5.2.1) for stars with IRS and/or 70 μm excesses. Refer to Figure 9 for error bars on the IRS data. Measured spectra are shown with solid lines, modeled spectra are shown with dashed lines. "I" indicates the star has an IRS excess, "M" indicates the star has a MIPS 70 μm excess, and a "w" indicates that the excess is weak.

R_1, and R_2, we were able to minimize the reduced χ^2 to values between 0.6 and 1.2, except for HD 10647, which has a fit with a reduced χ^2 of 5.7, indicating a simple 10 μm dust grain model does not satisfactorily fit the infrared excess observed for this star (see Sections 5.2.2 and 5.2.3). Results of the model fitting are shown in Figure 12 and Table 7 and are discussed below.

Mass estimates are notoriously tricky to derive given uncertainties in grain sizes. Assuming a silicate grain density of 3.3 g cm^{-3}, we calculate dust masses of 4×10^{-7}–2.4×10^{-3} $M_\oplus$. Extrapolating this estimate using the -3.5 index power law appropriate for a distribution of sizes from a collisional cascade (Dohnanyi 1969) up to a maximum size of 10 km yields total mass estimates as shown in Table 7. Submillimeter observations of all these sources would further constrain the dust size and distribution and thus the total mass of the emitting material.

$L_{\rm dust}/L_\star$ values were obtained by integrating the excess over frequency, including a power-law interpolation between 35 and 70 μm (if available). We used a simple blackbody curve to extrapolate beyond 70 μm, based on the middle of the temperature range found by the model and quoted in Table 7. For stars with a 70 μm excess only, we used Equation (1) at 70 μm.

The models match the spectra quite well (Figure 12), yielding dust temperatures between ∼50 and 450 K (Figure 13) and dust locations between ∼1 and 35 AU (Figure 14). The majority of disks are located between 10 and 30 AU from their stars with several (∼7/19) showing a single temperature fit perhaps indicative of a ring-like structure that may be found with higher resolution data. Since the IRS data place only a limit on the emission shortward of 34 μm for HD 90089, HD 132254, and HD 160032, the single grain model can be used to show that the inner edge of the disk seen at 70 μm must start beyond ∼15 AU corresponding to material cooler than ∼70 K. The mean value of the disk sizes shown in Figure 14 is 14 $\pm$ 6 AU.

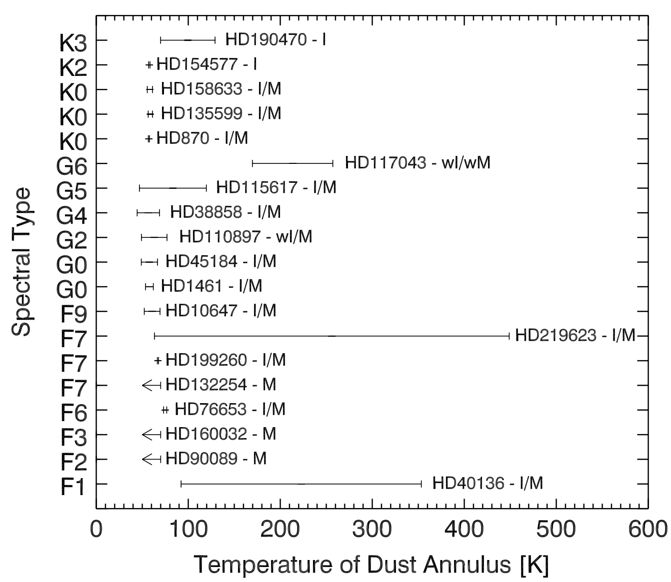

Figure 13. Calculated dust temperatures based on model spectra (Table 7; Figure 12). Stars are arranged by spectral type. "I" indicates the star has an IRS excess, "M" indicates the star has a MIPS 70 μm excess, and a "w" indicates that the excess is weak.

Table 7
Large Dust Models

Star	Excess	Spectral Type	$R_1 - R_2$ (AU)	$T_1 - T_2$ (K)	Reduced χ^2	Optical Depth τ (10 μm)	$M_{\rm grain}$[a] ($M_\oplus$)	($M_\oplus$ < 10 km)	$L_{\rm dust}/L_\star$[b] (10^{-7})
HD 870	IRS and MIPS 70 μm	K0V	12 − 12	58 − 57	0.8[c]	1.5×10^{-3}	7.8×10^{-6}	0.2	245 ± 91
HD 1461	IRS and MIPS 70 μm	G0V	19 − 26	62 − 54	0.9[c]	2.7×10^{-4}	3.4×10^{-5}	1.06	343 ± 45
HD 10647	IRS and MIPS 70 μm	F9V	16 − 29	69 − 52	5.7[d]	10.0×10^{-4}	2.4×10^{-4}	7.7	2627 ± 118[e]
HD 38858	IRS and MIPS 70 μm	G4V	12 − 29	69 − 44	1.0[c]	1.7×10^{-4}	5.3×10^{-5}	1.7	677 ± 141
HD 40136	IRS and MIPS 70 μm	F1V	1 − 16	353 − 92	0.8[d]	1.1×10^{-5}	1.2×10^{-6}	0.039	62 ± 14
HD 45184	IRS and MIPS 70 μm	G2IV	11 − 27	77 − 49	1.2[d]	2.0×10^{-4}	5.3×10^{-5}	1.68	810 ± 89
HD 76653	IRS and weak MIPS 70 μm	F6V	16 − 18	77 − 73	0.9[c]	4.7×10^{-4}	1.0×10^{-5}	0.33	164 ± 47
HD 90089	IRS limit and MIPS 70 μm	F2V	>15	<70	0.8[c]	...	...	...	167 ± 21
HD 110897	Weak IRS and MIPS 70 μm	G0V	17 − 31	67 − 49	0.9[c]	5.5×10^{-5}	1.6×10^{-5}	0.50	187 ± 34
HD 115617	IRS and MIPS 70 μm	G5V	4 − 25	120 − 47	0.7[d]	3.1×10^{-5}	8.1×10^{-6}	0.26	199 ± 39[f]
HD 117043	Weak IRS and weak MIPS 70 μm	G6V	1 − 2	257 − 170	1.1[d]	3.4×10^{-5}	3.8×10^{-8}	0.0012	69 ± 21
HD 132254	IRS limit and MIPS 70 μm	F7V	>15	<70	0.7[c]	...	...	...	208 ± 62
HD 135599	IRS and MIPS 70 μm	K0	11 − 12	61 − 56	0.7[c]	1.3×10^{-3}	2.4×10^{-5}	0.77	994 ± 84
HD 154577	IRS and MIPS 70 μm limit	K2V	10 − 10	58 − 57	0.7[c]	8.4×10^{-4}	3.6×10^{-6}	0.1	104 ± 70
HD 158633	IRS and MIPS 70 μm	K0V	11 − 13	61 − 55	0.8[c]	3.5×10^{-4}	8.1×10^{-6}	0.26	299 ± 53
HD 160032	IRS limit and MIPS 70 μm	F3IV	>15	<70	0.6[c]	...	...	...	320 ± 94
HD 190470	IRS, poor MIPS data[g]	K3V	2 − 6	129 − 70	0.8[d]	9.7×10^{-5}	1.4×10^{-6}	0.044	307 ± 43
HD 199260	IRS and MIPS 70 μm	F7V	19 − 20	68 − 66	1.0[d]	8.4×10^{-4}	1.1×10^{-5}	0.34	177 ± 34
HD 219623	IRS and MIPS 70 μm	F7V	0.4 − 22	449 − 63	1.1[d]	1.4×10^{-5}	3.0×10^{-6}	0.09	136 ± 22

Notes.
[a] Calculated assuming 10 μm dust grains.
[b] See note in Section 5.2.1 for how $L_{\rm dust}/L_\star$ is calculated.
[c] $\lambda > 21$ μm, 74 dof.
[d] $\lambda > 14$ μm, 152 dof.
[e] Tanner et al. (2009) calculate $L_{\rm dust}/L_\star = 2770 \times 10^{-7}$ including the MIPS 160 μm data point.
[f] Tanner et al. (2009) calculate $L_{\rm dust}/L_\star = 259 \times 10^{-7}$ including the MIPS 160 μm datapoint.
[g] This star is located in a particularly noisy field, so the model is fit to the IRS data only, and $L_{\rm dust}/L_\star$ is calculated using data out to 35 μm only.

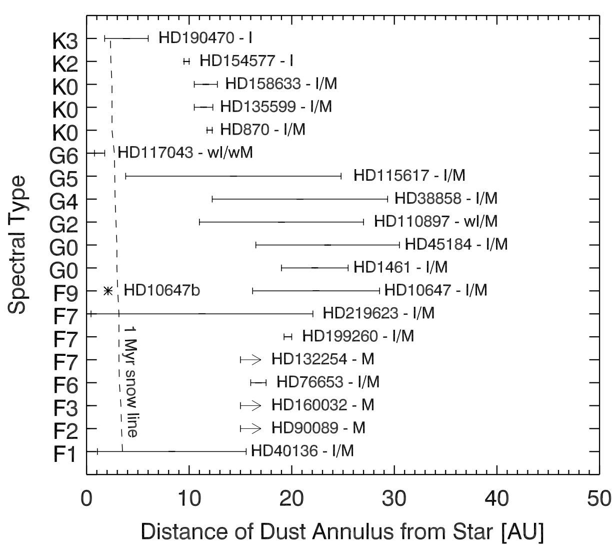

Figure 14. Calculated dust radii based on model spectra (Table 7; Figure 12). Stars are arranged by spectral type. "I" indicates the star has an IRS excess, "M" indicates that the star has a MIPS 70 μm excess, and a "w" indicates that the excess is weak. Also noted on this plot is the theoretical 1 Myr snow line (based on Siess et al. 2000) and the location of HD 10647's known planet.

It is important to note, however, that these disk sizes are crucially dependent on the assumed grain size and that, as discussed below, smaller grains could dramatically increase the distance at which the emitting grains are actually located (e.g., G. Bryden et al., in preparation).

5.2.2. More Complex Dust Models

While models using single population of 10 μm dust grains reproduce the weak, featureless spectra of most of our stars with excesses, we tried to model some of the excesses using a more realistic mixture of grains of different sizes and material compositions. The compositional model applied to HD 69830 (Lisse et al. 2007) and HD 113766 (Lisse et al. 2008) utilizes a combination of water ice, amorphous and crystalline olivine, and amorphous and crystalline pyroxene. The mix used here contains roughly 50:50 rocky dust and water ice, similar to the abundances seen in the small icy bodies of the Kuiper Belt, but of the 152 program stars, only two (HD 10647 and HD 40136) show hints for spectral features around 20 μm and neither of these stars has a statistically significant IRS excess shortward of 18 μm, severely hampering the fitting due to the lack of emission features available to constrain the models. The remainder of the stars did not offer enough statistically significant data to merit more sophisticated modeling than the simple characterization described in Section 5.2.1.

Applying the compositional model to HD 40136, we were able to derive good, although relatively unconstrained fits to the 18–35 μm IRS data, finding evidence for crystalline olivine (50:50 Fe/Mg-rich), crystalline pyroxene, FeS and some water ice, with a reduced $\chi^2 \sim 0.8$ (Figure 15). Removing silicates worsened the fit to a reduced $\chi^2 \sim 1.6$, mostly due to a failure to fit the data around the 18–20 μm silicate feature. However, the S/N is poor shortward of 20 μm due to the bright stellar photosphere, making these identifications preliminary.

The model for HD 10647 yields a similar mix of ices and silicates, with a reduced $\chi^2 \sim 0.8$ (Figure 15). Removing silicates from the fit gives a significantly worse reduced $\chi^2 \sim 56$, strongly supporting the inclusion of silicates in the model spectrum. This model is discussed further in Tanner et al. (2009).

Because of the low S/N shortward of 18 μm for both of these stars, identification of minerals will have to await future observations. The *Herschel Space Observatory* could prove

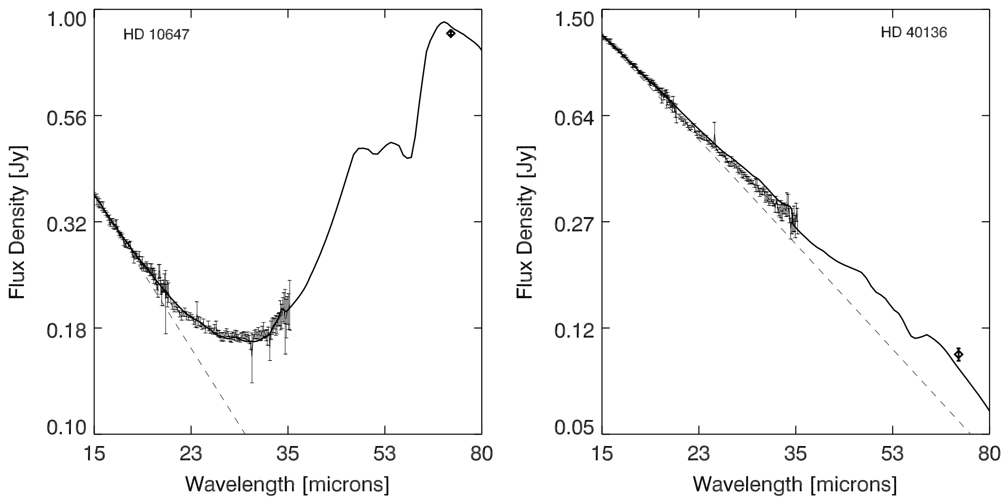

Figure 15. Results of the mineralogical model discussed in Section 5.2.2, using a combination of water ice and silicates. The dashed line shows the spectrum of the stellar photosphere, while the solid line shows the model. Also shown are the IRS spectra and the MIPS 70 μm data point.

especially useful to check for the evidence of a water ice feature near 62 μm (Figure 15).

5.2.3. Stars with Observed Extended Emission

HD 10647, HD 38858, and HD 115617 are all marginally extended in their MIPS 70 μm images. When dust rings are fit to this extended emission, G. Bryden et al. (2009, in preparation) find much larger radii (∼100 AU) than indicated by our models. This can be explained by either different grain emissivities, or by two populations of dust grains: larger, 10 μm dust grains in a closer annulus (∼10–30 AU), and smaller dust grains at larger radii (∼100 AU)

HD 10647 and HD 115617 are also detected in MIPS 160 μm images (Tanner et al. 2009), further supporting the hypothesis of two dust populations. At 160 μm, emission from the stellar photosphere is negligible, so the detected emission is attributed to cold (∼30 K) dust at large distances (∼100 AU) from the star, much farther out than our model based on the warm dust predicts.

The case of the planet-bearing star HD 10647 is particularly interesting since not only is it detected at 160 μm and resolved at 70 μm, but its disk is also resolved in coronagraphic images from the Advanced Camera for Surveys on the *Hubble Space Telescope* (Stapelfeldt et al. 2007). Its very high $L_{\rm dust}/L_\star$ and young age make this the most likely star in our sample to have small grains due to a recent collisional event. A compositional model (as used in Section 5.2.2) incorporating an additional population of very cold, small grains composed primarily of water ice fits the combined data sets very well. The data and the relevant model are discussed in depth in Tanner et al. (2009).

5.3. Characteristics of the Dust

Only three stars have convincing evidence for warm dust: HD 40136, HD 190470, and HD 219623. One star, HD 117043, has hints of warm excess but is too weak at both IRS and MIPS for further consideration. HD 40136 and HD 219623 have MIPS excesses as well, while HD 190470 has significant cirrus contamination so the MIPS limit is poor. The simple model (Section 5.2.1) for HD 40136 and HD 219623 shows material extending to within 1 AU (Figure 14), suggestive of disks with active reprocessing of material, given the short grain lifetimes at these small orbital radii (Wyatt 2008).

All of the remaining stars with excesses have their emitting material located in regions analogous to the Kuiper Belt in our solar system, typically beyond 10 AU, out to a maximum value of 30 AU (Figure 14). In the two cases where the signal-to-noise ratio is (barely) adequate for mineralogical analysis, HD 10647 (Section 5.2.2 and Tanner et al. 2009) and HD 40136 (Section 5.2.2), the suggestion of significant amounts of water ice is intriguing and is to be expected for regions that lie well beyond the snow line, where volatiles are predicted to be abundant (Pollack et al. 1996). Figure 14 shows the location of the snow line for 1 Myr old stars (using stellar models from Siess et al. 2000), an age when stellar luminosity and the volatile content of the outer disk should be stabilizing. The majority of our sample have material located at or well beyond the snow line.

The total quantity of material responsible for the observed excesses is poorly constrained by our data, because of uncertainties in grain properties and in the extrapolation up to maximum particle size. Table 7 lists total masses extrapolating a population of bodies with 3.3 g cm^{-3} and a $N(a) \propto a^{-3.5}$ size distribution up to 10 km. The median value for 13 stars with strong IRS and MIPS excesses is 0.34 $M_\oplus$. The average and standard deviation, 1.0 $\pm$ 2.1 $M_\oplus$, are dominated by a few outliers with more massive disks: HD 1461, HD 38858, and HD 45184 all around 1–2 $M_\oplus$, and especially HD 10647 with an extrapolated total mass of 7.7 $M_\oplus$. These mass estimates can be compared to various estimates for the mass of our own Kuiper Belt or to models of the primitive solar nebula. In the Nice model of outer solar system formation, for example, the outer disk contains roughly 10–150 $M_\oplus$ of material in bodies with densities of 1 g cm^{-3} in sizes up to 300 km (Alessandro et al. 2009). It is difficult to compare these values directly to ours, since we assumed a smaller maximum size, 10 km versus 300 km for Alessandro et al. (2009). However, this is offset by our different density assumptions: we assumed 3.3 g cm^{-3}, while Alessandro et al. (2009) used 1 g cm^{-3}. More importantly, our 18–70 μm data are probably missing significant emission from other populations of dust: more distant and/or larger grains would emit at longer wavelengths. On the other hand, the order of magnitude agreement between our measurements and an existing solar system model is encouraging.

It should be noted, however, that the stars with strong excesses are in the minority of our sample (<12%) and that the vast majority of the mature stars in our study (and other *Spitzer* studies) have Kuiper Belt disk masses less than 0.1 $M_\oplus$, the approximate mass of the Kuiper Belt in our solar system (Gladman et al. 2001). This relatively strict upper limit must eventually be reconciled with the presence or absence of gas giant or icy giants in the outer reaches of planetary systems.

6. CONCLUSION

We have used the IRS instrument on the *Spitzer Space Telescope* to look for excesses around nearby, solar-type stars. We find that none of our 152 sample stars have significant excesses in the 8.5–12 μm portion of the spectrum, while 16 have excesses beginning at $\sim$15–25 μm and rising to longer wavelengths. Including stars that meet our sample criteria and were previously observed with the IRS instrument, we find that 11.8% $\pm$ 2.4% of nearby, solar-type stars have excesses at 30–34 μm, while only 1.0% $\pm$ 0.7% have excesses at 8.5–12 μm. The rarity of short-wavelength excesses is consistent with models (Wyatt et al. 2007); for ages older than 1 Gyr, disks should fall below our sensitivity threshold. Bright emission such as that seen toward HD 69830 must be intrinsically rare, have a duty cycle less than 1% of the typical 2 Gyr age of these stars, or an occurrence less than once per 20 million years. This could mean that the habitable zones of nearby solar-type stars have a very low incidence of massive collisions, providing opportunity for stable, catastrophe-free terrestrial planets.

This publication makes use of data products from the Two-Micron All Sky Survey, as well as from IPAC/IRSKY/IBIS, SIMBAD, VizieR, the ROE Debris Disks Database website, and the Extrasolar Planets Encyclopaedia website. The *Spitzer Space Telescope* is operated by the Jet Propulsion Laboratory, California Institute of Technology, under NASA contract 1407. Development of MIPS was funded by NASA through the Jet Propulsion Laboratory, subcontract 960785. Some of the research described in this publication was carried out at the Jet Propulsion Laboratory, California Institute of Technology, under a contract with the National Aeronautics and Space Administration. S.M.L. thanks Seth Redfield and Roy Kilgard for very helpful comments and advice regarding this paper.

APPENDIX

IRS DATA FOR STARS WITH EXCESS

Complete IRS data for all 16 stars with excesses in these wavelengths are presented in Table 8 below.

Table 8
HD 870

Wavelength (μm)	F_ν (Jy)	Excess (Jy)	Fractional Excess
7.576	0.4784	−0.0020 $\pm$ 0.0046	−0.0043 $\pm$ 0.0097
7.637	0.4721	−0.0006 $\pm$ 0.0048	−0.0014 $\pm$ 0.0102
7.697	0.4692	0.0038 $\pm$ 0.0052	0.0082 $\pm$ 0.0110
7.758	0.4583	−0.0004 $\pm$ 0.0094	−0.0009 $\pm$ 0.0204
7.818	0.4536	0.0018 $\pm$ 0.0054	0.0039 $\pm$ 0.0118
7.878	0.4400	−0.0052 $\pm$ 0.0036	−0.0119 $\pm$ 0.0081
7.939	0.4430	0.0043 $\pm$ 0.0051	0.0098 $\pm$ 0.0114
7.999	0.4382	0.0061 $\pm$ 0.0048	0.0138 $\pm$ 0.0109
8.060	0.4201	−0.0053 $\pm$ 0.0042	−0.0126 $\pm$ 0.0100

(A supplementary tar file is available in the online journal.)

REFERENCES

Absil, O., et al. 2006, A&A, 452, 237
Backman, D. 2004, in ASP Conf. Ser. 324, Debris Disks and the Formation of Planets, ed. L. Caroff et al. (San Francisco, CA: ASP), 9
Backman, D. E., & Paresce, F. 1993, in Protostars and Planets III, ed. E. H. Levy & J. I. Lumine (Tucson, AZ: Univ. Arizona Press), 1253
Barry, D. C. 1988, ApJ, 334, 436
Beichman, C. A., Fridlund, M., Traub, W. A., Stapelfeldt, K. R., Quirrenbach, A., & Seager, S. 2007, in Protostars and Planets V, ed. V, B. Reipurth, D. Jewitt, & K. Keil (Tucson, AZ: Univ. of Arizona Press), 915
Beichman, C. A., et al. 2005a, ApJ, 622, 1160
Beichman, C. A., et al. 2005b, ApJ, 626, 1061
Beichman, C. A., et al. 2006a, ApJ, 639, 1166
Beichman, C. A., et al. 2006b, ApJ, 652, 1674
Bertone, E., Buzzoni, A., Chávez, M., & Rodríguez-Merino, L. H. 2004, AJ, 128, 829
Borges, A. C., Idiart, T. P., de Freitas Pacheco, J. A., & Thevenin, F. 1995, AJ, 110, 2408
Borkova, T. V., & Marsakov, V. A. 2005, VizieR Online Data Catalog, 808, 20453
Bryden, G., et al. 2006, ApJ, 636, 1098
Buitrago, J., & Mediavilla, E. 1985, A&A, 148, L8
Burns, J. A., Lamy, P. L., & Soter, S. 1979, Icarus, 40, 1
Butler, R. P., et al. 2006, ApJ, 646, 505
Carpenter, J. M., et al. 2008, ApJS, 179, 423
Cayrel de Strobel, G., Soubiran, C., Friel, E. D., Ralite, N., & Francois, P. 1996, VizieR Online Data Catalog, 3200, 0
Cayrel de Strobel, G., Soubiran, C., & Ralite, N. 2001, VizieR Online Data Catalog, 3221, 0
Cenarro, A. J., Cardiel, N., Gorgas, J., Peletier, R. F., Vazdekis, A., & Prada, F. 2001, VizieR Online Data Catalog, 732, 60959
Chen, C. H., et al. 2006, ApJS, 166, 351
Chen, Y. Q., Nissen, P. E., Benoni, T., & Zhao, G. 2001, VizieR Online Data Catalog, 337, 10943
Ciardi, D. R., van Belle, G. T., Akeson, R. L., Thompson, R. R., Lada, E. A., & Howell, S. B. 2001, ApJ, 559, 1147
Dermott, S. F., Kehoe, T. J. J., Durda, D. D., Grogan, K., & Nesvorný, D. 2002, in Proc. Asteroids, Comets, and Meteors: ACM2002, ed. B. Warmbein (ESA-SP 500; Noordwijk: ESA Publications Division), 319
Dohnanyi, J. S. 1969, J. Geophys. Res., 74, 2431
Draine, B. T., & Lee, H. M. 1984, ApJ, 285, 89
Ducati, J. R. 2002, VizieR Online Data Catalog, 2237, 0
Eggen, O. J. 1998, AJ, 115, 2397
Engelbracht, C. W., et al. 2007, PASP, 119, 994
Fajardo-Acosta, S. B., Telesco, C. M., & Knacke, R. F. 1993, ApJ, 417, L33
Feltzing, S., Holmberg, J., & Hurley, J. R. 2001, VizieR Online Data Catalog, 337, 70911
Gautier, T. N., III, et al. 2007, ApJ, 667, 527
Gladman, B., Kavelaars, J. J., Petit, J. M., Morbidelli, A., Holman, M. J., & Loredo, T. 2001, AJ, 122, 1051
Gordon, K. D., et al. 2005, PASP, 117, 503
Gordon, K. D., et al. 2007, PASP, 119, 1019
Hauschildt, P. H., Allard, F., & Baron, E. 1999a, ApJ, 512, 377
Hauschildt, P. H., Allard, F., Ferguson, J., Baron, E., & Alexander, D. R. 1999b, ApJ, 525, 871
Hillenbrand, L. A., et al. 2008, ApJ, 677, 630
Houck, J. R., et al. 2004, ApJS, 154, 18
Ibukiyama, A., & Arimoto, N. 2002, VizieR Online Data Catalog, 339, 40927
Johnson, H. L., Mitchell, R. I., & Iriarte, B. 2001, VizieR Online Data Catalog, 2005, 0
Jura, M., et al. 2004, ApJS, 154, 453
Kalas, P., et al. 2008, Science, 322, 1345
Kidger, M. R., & Martín-Luis, F. 2003, AJ, 125, 3311
Kurucz, R. L. 1992, in IAU Symp. 149, The Stellar Populations of Galaxies, ed. B. Barbuy & A. Renzini (Dordrecht: Kluwer), 225
Lachaume, R., Dominik, C., Lanz, T., & Habing, H. J. 1999, A&A, 348, 897
Lambert, D. L., & Reddy, B. E. 2004, VizieR Online Data Catalog, 734, 90757
Lebreton, Y., Perrin, M.-N., Cayrel, R., Baglin, A., & Fernandes, J. 1999, A&A, 350, 587
Lisse, C. M., Beichman, C. A., Bryden, G., & Wyatt, M. C. 2007, ApJ, 658, 584
Lisse, C. M., Chen, C. H., Wyatt, M. C., & Morlok, A. 2008, ApJ, 673, 1106
Lovis, C., et al. 2006, Nature, 441, 305
Marois, C., Macintosh, B., Barman, T., Zuckerman, B., Song, I., Patience, J., Lafrenière, D., & Doyon, R. 2008, Science, 322, 1348

Marsakov, V. A., & Shevelev, Y. G. 1988, Bull. Inf. Cent. Donnees Stellaires, 35, 129
Marsakov, V. A., & Shevelev, Y. G. 1995, VizieR Online Data Catalog, 5089, 0
Mashonkina, L., & Gehren, T. 2001, A&A, 376, 232
Mayor, M., et al. 2003, 19th IAP Colloquium, Paris, June 2003
Mayor, M., et al. 2009, A&A, 493, 639
Morbidelli, A., Levison, H. F., Bottke, W., Dones, L., & Nesvorny, D. 2009, arXiv:0903.0923
Morel, M., & Magnenat, P. 1978, A&AS, 34, 477
Nitschelm, C., Lecavelier des Etangs, A., Vidal-Madjar, A., Ferlet, R., Olsen, E. H., & Dennefeld, M. 2000, A&AS, 145, 275
Nordström, B., et al. 2004, A&A, 418, 989
Perrin, M.-N., de Strobel, G. C., Cayrel, R., & Hejlesen, P. M. 1977, A&A, 54, 779
Plavchan, P., Werner, M. W., Chen, C. H., Stapelfeldt, K. R., Su, K. Y. L., Stauffer, J. R., & Song, I. 2009, ApJ, 698, 1068
Pollack, J. B., Hubickyj, O., Bodenheimer, P., Lissauer, J. J., Podolak, M., & Greenzweig, Y. 1996, Icarus, 124, 62
Randich, S., Gratton, R., Pallavicini, R., Pasquini, L., & Carretta, E. 1999, A&A, 348, 487
Reach, W. T., Morris, P., Boulanger, F., & Okumura, K. 2003, Icarus, 164, 384
Rhee, J. H., Song, I., Zuckerman, B., & McElwain, M. 2007, ApJ, 660, 1556
Rieke, G. H., et al. 2004, ApJS, 154, 25
Rieke, G. H., et al. 2008, AJ, 135, 2245
Rocha-Pinto, H. J., & Maciel, W. J. 1998, MNRAS, 298, 332
Siegler, N., Muzerolle, J., Young, E. T., Rieke, G. H., Mamajek, E. E., Trilling, D. E., Gorlova, N., & Su, K. Y. L. 2007, ApJ, 654, 580
Siess, L., Dufour, E., & Forestini, M. 2000, A&A, 358, 593
Song, I., Zuckerman, B., Weinberger, A. J., & Becklin, E. E. 2005, Nature, 436, 363
Stapelfeldt, K., Krist, J., Bryden, G., & Chen, C. 2007, in Proc. Conf. In the Spirit of Bernard Lyot: The Direct Detection of Planets and Circumstellar Disks in the 21st Century, ed. P. Kalas, 47
Stapelfeldt, K. R., et al. 2004, BAAS, 36, 700
Stern, S. A. 1996, A&A, 310, 999
Su, K. Y. L., et al. 2005, ApJ, 628, 487
Su, K. Y. L., et al. 2006, ApJ, 653, 675
Sylvester, R. J., & Mannings, V. 2000, MNRAS, 313, 73
Tanner, A., Beichman, C., Bryden, G., Lisse, C., & Lawler, S. 2009, ApJ, 704, 109
Taylor, B. J. 2003, A&A, 398, 731
Telesco, C. M., & Knacke, R. F. 1991, ApJ, 372, L29
Thevenin, F. 1998, VizieR Online Data Catalog, 3193, 0
Trilling, D. E., et al. 2008, ApJ, 674, 1086
Udry, S., et al. 2006, A&A, 447, 361
Valenti, J. A., & Fischer, D. A. 2005, ApJS, 159, 141
Weingartner, J. C., & Draine, B. T. 2001, ApJ, 548, 296
Wooden, D. H., Butner, H. M., Harker, D. E., & Woodward, C. E. 2000, Icarus, 143, 126
Wright, J. T., Marcy, G. W., Butler, R. P., & Vogt, S. S. 2004, ApJS, 152, 261
Wright, J. T., Marcy, G. W., Butler, R. P., Vogt, S. S., Henry, G. W., Isaacson, H., & Howard, A. W. 2008, ApJ, 683, L63
Wyatt, M. C. 2008, ARA&A, 46, 339
Wyatt, M. C., Smith, R., Greaves, J. S., Beichman, C. A., Bryden, G., & Lisse, C. M. 2007, ApJ, 658, 569
Zuckerman, B., & Song, I. 2004, ApJ, 603, 738